Evaluation of vertically resolved longwave radiation in SPARTACUS-~~Surface~~Urban 0.7.3 and the sensitivity to urban surface temperatures

Megan A. Stretton[1], William Morrison[1,2], Robin J. Hogan[1,3], Sue Grimmond[1]~~,~~

[1]Department of Meteorology, University of Reading, Reading, UK
[2]Chair of Environmental Meteorology, Faculty of Environment and Natural Resources, University of Freiburg, Freiburg, Germany
[3]European Centre for Medium-Range Weather Forecasts, Reading, UK

Correspondence to: Megan A. Stretton (m.a.stretton@~~pgr.~~reading.ac.uk)

Abstract. Cities materials and urban form impact radiative exchanges, and ~~hence both~~ surface and air temperatures. Here, the 'SPARTACUS' multi-layer approach to modelling longwave radiation in urban areas (SPARTACUS-Urban) is evaluated using the explicit DART (Discrete Anisotropic Radiative Transfer) model. SPARTACUS-Urban describes realistic 3D urban geometry statistically, rather than assuming an infinite street canyon. Longwave flux profiles are compared across an August day for a 2 km x 2 km domain in central London. Simulations are conducted with multiple temperature configurations, including realistic temperature profiles derived from thermal camera observations. The SPARTACUS-Urban model performs well (cf. DART) when all facets are prescribed a single temperature, with normalised bias errors (nBE) < 2.5% for ~~longwave~~ downwelling ~~at the surface~~fluxes, and < 0.5% for ~~the~~top-of-canopy upwelling ~~longwave at the top of the canopy.~~fluxes. Errors are larger (nBE < 8%) for ~~the~~ net longwave fluxes from walls and roofs. Using more realistic surface temperatures, ~~which vary~~varying depending on ~~whether a~~ surface ~~is sunlit~~shading, the nBE in upwelling longwave increases to ~2%. Errors in roof and wall net longwave fluxes increase through the day, but ~~still~~ nBE are still 8–11%. This increase in nBE occurs because SPARTACUS-Urban represents vertical~~ variation of~~, but not horizontal, surface temperature ~~but not horizontal variations~~ variation within a domain. Additionally, SPARTACUS-Urban outperforms the Harman single-layer canyon approach, particularly in the longwave interception by roofs. We conclude that SPARTACUS-Urban accurately predicts longwave fluxes, requiring less computational time cf. DART, but with larger errors when surface temperatures vary ~~because of being sunlit and/or shaded.~~due to shading. SPARTACUS-Urban could enhance multi-layer urban energy balance schemes prediction of within-canopy temperatures and fluxes.

1 Introduction

The differences in energy exchanges between urban and rural areas leads to canopy layer air temperature differences of 3-10°C (Oke 1987). This phenomenon, known as the canopy layer urban heat island effect (CL-UHI), has been studied and observed worldwide (Oke 1982; Zhang et al. 2012; Wu et al. 2014; Guo et al. 2016; Dou and Miao 2017; Gaitani et al. 2017). The CL-UHI is driven by contrasting radiative exchanges between urban and rural environments, resulting from the heterogeneous nature of cities (Aida and Gotoh 1982; Oke 1982; Kondo et al. 2001; Harman and Belcher 2006; Ao et al.

Style Definition: Comment Text
Formatted: Font: 16 pt
Formatted: Font: 16 pt
Formatted: Tab stops: 15.68 cm, Left + Not at 10.74 cm
Formatted: English (United Kingdom)
Formatted: English (United Kingdom)
Formatted: Danish
Field Code Changed

2016). With increasing urbanization, and more people residing in cities than rural areas since 2007 (Heaviside et al. 2017), there is greater exposure of vulnerable people to extreme weather, such as heatwaves, with the severity of such events potentially exacerbated by the CL-UHI.

The heterogenous 3D structures of urban areas lead to changes in the surface energy balance, and diurnal temperatures (Souch and Grimmond 2006; Masson et al. 2008), due to the resultant differential shortwave (SW) input and radiative cooling across a city. The crenulated urban morphology and resultant deep canyons cause an uneven exposure to the sky and an increased ~~the~~ surface area available for exchange (cf. rural areas), which increases the SW absorption throughout the day. This differential solar irradiance drives temperature variations between facets, including vertical gradients (Oke 1981; Blankenstein and Kuttler 2004; Harman and Belcher 2006; Hénon et al. 2012; Hu and Wendel 2019).

The spatial variation of facet temperatures is highest during the daytime, due to variations in the absorption and reflection of the dynamic solar radiation (Myint et al. 2013; Crum and Jenerette 2017; Antoniou et al. 2019). However, temperatures remain high overnight from the morphology reducing exposure to the sky therefore increasing radiative trapping and slowing cooling rates, and ~~lower~~lowering effective albedo. Facet materials (e.g., concrete, tarmac) can have low albedo, high heat capacities and high thermal inertia (Bohnenstengel et al. 2011). This results in large daytime heat storage ~~in to~~into the urban volume, which is released slowly at night (Meyn and Oke 2009; Kershaw and Millward 2012).

These impacts on the radiative and other energy exchanges ~~needs~~need to be parameterised within ~~by the~~ numerical weather prediction (NWP) land surface schemes (Masson 2006). A common approach to simplifying the 3D structure of cities is to treat the urban form as a single canyon between buildings of equal height (Nunez and Oke 1977). Initially, in some standalone models, some complexity was considered ~~(,~~ e.g., allowing intersections~~)~~ (e.g., Aida 1982; Arnfield 1982a, 1988), when modelling urban radiative exchanges. But ~~for NWP~~, with NWP computer resource limitations~~, this was simplified to assuming~~ an infinite canyon~~, as it simplifies the~~ was assumed, simplifying view factor geometry and computations (e.g., Masson 2000; Harman et al. 2004), an approach which ~~is also used~~has been adopted for ~~the~~ other energy balance fluxes (e.g., Masson 2000; Kusaka et al. 2001a; Lee and Park 2008). Many of these models calculate the fluxes for individual facets (wall, roof, and ground) (Masson 2006). However, assuming ~~the~~a constant building height and lack of intersections neglects the variability of urban geometry (e.g., clusters of tall buildings, courtyards) that influence shadowing and trapping of radiation, and wind fields (e.g., Hertwig et al. 2019, 2021).

Sub-facet differences (e.g., roof orientation, and slopes, high/low parts of walls, wall orientation, sunlit/shaded pavement) can create surface temperature variability, which is not ~~-~~ captured if represented by a single mean surface temperature in an urban energy balance scheme (Hilland and Voogt 2020). For example, diurnal variations of wall temperature are linked to their orientation relative to the sun, and additionally to inter-building interactions (e.g. shadows) (Nazarian and Kleissl 2015;

Formatted: Danish

Formatted: English (United Kingdom)

Field Code Changed

Formatted: English (United Kingdom)

Antoniou et al. 2019). This is important as 12-50% of the urban surface is comprised of walls (Voogt et al. 1997; Grimmond and Oke 1999; Hénon et al. 2012). Similarly, roofs differ from walls, with high incident SW radiation (Harman and Belcher 2006; Morrison et al. 2018), and ground surfaces in deep urban canyons may have dampened diurnal temperature variability (Hu and Wendel 2019). Inclusion of the vertical variability of the urban form may allow such features to be captured by models, unlike within the infinite homogenous canyon approach.

Some of these features can be addressed by utilising multi-layer radiative transfer models, allowing more nuanced radiative trapping and realistic vertical temperature distributions (e.g.~~,~~, Seoul National University Canopy Model (Ryu and Baik 2012; Ryu et al. 2013)~~, and SPARTACUS-Urban (Hogan 2019)), which allow for variations in roof and wall heights. This leads to more nuanced radiative trapping and more realistic vertical temperature distributions. The SPARTACUS-Urban model uses vertical profiles of urban geometry to simulate radiation between buildings to account for atmospheric absorption, emission, and scattering, whilst being fast enough to be used for NWP. Wall and roof areas are derived from building footprint data but can be simplified to two parameters. The shortwave (SW) capabilities, evaluated using an explicit radiative transfer model, are in good agreement for realistic urban domains (Stretton et al. 2022).~~

, Building Effect Parameterisation (BEP, Martilli et al. (2002); Schubert et al. (2012)), the Town Energy Balance model (TEB, Hamdi and Masson (2008)), and SPARTACUS-Urban (Hogan 2019a)). Most assume a canyon geometry, those with varying building heights permitting more realistic inter-building shading (e.g., Schubert et al. (2012)). SPARTACUS-Urban assumes buildings are distributed randomly in the horizontal plane, with geometry describable by vertical profiles of building plan area and building edge length, allowing radiative exchanges simulations fast enough for NWP accounting for atmospheric absorption, emission, and scattering between buildings. The approach provides a more accurate description of radiation exchange than single layer street-canyon approaches (Hogan 2019b). The shortwave (SW) simulations for realistic urban domains have good agreement to an explicit radiative transfer model (Stretton et al. 2022).

In this study, the longwave (LW) capabilities ~~of SPARTACUS-Urban~~ are evaluated for the first time~~, using both~~. SPARTACUS-Urban's performance is compared to both the explicit scheme DART (Discrete Anisotropic Radiative Transfer ~~(Gastellu-Etchegorry et al. 2015) and the Harman et al. (2004) models (Sect. 2). The former is an explicit scheme. The latter takes~~, Gastellu-Etchegorry et al. (2015)) and to a common approach used in operational ~~weather and climate models. We~~NWP and climate modelling, Harman et al. (2004) (Sect. 2). To examine SPARTACUS-Urban's ~~prediction of~~ LW fluxes ~~for a domain~~we simulate an area in central London, with ~~varying complexities of~~ facet temperatures ~~derived~~available from thermal camera observations (Morrison et al. 2020, 2021) ~~to undertake~~that can be prescribed with varying levels of complexity for the evaluation (Sect. 3). ~~A comparison~~Comparison of SPARTACUS-Urban ~~and~~to DART ~~is made~~ (Sect. 4) and ~~with the~~to Harman et al. (2004) street canyon radiation (Sect. 5~~). The~~) is made, with the results ~~of the evaluation are~~ presented ~~(~~in Sect. 6~~)~~.

Formatted: English (United Kingdom)

Formatted: Font color: Text 1

Formatted: Font color: Text 1

Formatted: Font color: Text 1

Formatted: Font color: Text 1

Formatted: Font color: Text 1

2 Radiative transfer models

2.1 SPARTACUS-Urban

The SPARTACUS approach, developed to model radiative exchange within cloud fields (Hogan et al. 2016), has been applied to both vegetated ~~(Hogan et al. 2018)~~(Hogan et al. 2018) and built areas ~~(Hogan 2019b).~~(Hogan 2019a). Obstacles to radiation are assumed to be randomly distributed within the horizontal plane~~ to radiation~~, allowing simulation of a mean radiation field with height. ~~Although~~We use SPARTACUS-Surface open-source software (Hogan 2021) which includes both SPARTACUS-Urban and SPARTACUS-Vegetation~~, given~~. Given our buildings focus (i.e., excluding urban vegetation), we refer to this as “SPARTACUS-Urban”. ~~We previously~~Previously, we used DART to evaluate ~~SW part of~~ SPARTACUS-Urban SW for multiple urban geometry configurations ~~(Stretton et al. 2022)~~(Stretton et al. 2022).

A discrete-ordinate method is used to solve coupled ordinary-differential equations for 2*N* radiation streams (*N* streams per hemisphere, here $N = 8$). Radiative fluxes are calculated per height interval, *z*, for layers split into clear-air and building ‘regions’ in the horizontal plane. The incoming and outgoing fluxes (W m^{-2}), and absorption (W m^{-3}) profiles are calculated for three facets (wall, roof, and ground). SPARTACUS-Urban ~~requires profiles information for~~characterises each ~~scene (i.e., geometry~~model grid cell simulated using its morphology, emissivity (ε), and surface temperature (*T*~~) provided as~~). For morphology the plan area fraction (λ_p), building edge length (*L*), are required as a vertical profile that varies with height~~,~~ (*z*~~.~~). These, ~~and~~like other~~,~~ morphology parameters, can be derived from building footprint data (Martilli 2009; Kent et al. 2019; Stretton et al. 2022). SPARTACUS-Urban allows vertical variation of facet temperatures to be prescribed with one facet *T* per height level.

Although we assume a vacuum, SPARTACUS-Urban can account for atmospheric absorption. For this paper, we assume a wavelength of 10 μm (where atmospheric absorption is weak), so the emission rate in SPARTACUS-Urban (and DART) ~~make~~makes use of the Plank function at 10 μm, with a top-of-canopy downwelling longwave spectral flux at that wavelength (LW↓).

2.2 DART

The DART (Discrete Anisotropic Radiative Transfer) model (Gastellu-Etchegorry et al. 2015)~~ simulates the~~ can simulate variability of radiative exchanges ~~of radiation~~across one SPARTACUS-Urban grid cell in ~~heterogenous scenes. Scenes are imported as~~ detail using a 3D ~~models which can contain~~ digital surface model (DSM) with vegetation~~ and~~, buildings ~~(simulated as turbid media and planar triangle facets, respectively), with varying topography and a within-canopy~~ and atmosphere. ~~These scene elements interact with radiation iteratively within~~ Each voxel (or grid box) size has a ~~3D array of voxels. Scene elements~~user-prescribed resolution. The model domain's elements (e.g., vegetation, buildings) within a ~~given~~ voxel can interact with each other~~, and~~. The per-voxel ~~fluxes~~radiative budget products are stored after each ~~iteration.~~ numerical iteration. DART

Formatted: Danish

Formatted: Danish

Field Code Changed

scene elements are often represented by flat 'triangles' making up building walls and roofs or leaves on trees. Each triangle has an area, orientation, and optical properties. Alternatively, DART can represent vegetation as 'turbid media' (or volumes filled with randomly distributed infinitely small facets) characterised by an angular distribution and an area volume density.

To model the urban LW ~~exchanges~~field in DART, both a 3D building model and a ~~full~~ 3D field of surface temperatures ~~(prescribed to the triangles)~~ are ~~needed~~required. The latter can be ~~determined by~~ prescribed based on solar irradiance~~. DART's planar triangles can only~~ state (e.g., currently sunlit, shaded). Here, each building's triangles are categorised based on facet type (e.g., roof, wall) and orientation (e.g., west, east) to allow realistic spatial values. As a triangle can have only one ~~*T*, therefore~~temperature, if a ~~single~~ triangle covers ~~the full~~a whole wall (i.e., vertical ~~extent of a~~ building facet~~, it will only have one temperature to describe the~~) there is no vertical variation.

Formatted: Line spacing: single

~~DART has been evaluated using observations for vegetation (Sobrino et al. 2011) and relative to other models~~Given DART is an explicit radiative transfer model it has more detailed radiative interactions than the simpler radiative transfer models (e.g., SPARTACUS, Harman). DART has been evaluated in vegetated areas using thermal infrared observations (Sobrino et al. 2011) and relative to other models in the RAMI intercomparison project (Widlowski et al. 2015). ~~It has been applied in urban areas (e.g., Landier et al. 2018; Chrysoulakis et al. 2018; Morrison et al. 2020) and used for evaluations of simpler radiative transfer models (e.g., SPARTACUS-Urban, Stretton et al. (2022)~~The DART version including buildings (Gastellu-Etchegorry et al. 2015) has not been explicitly evaluated in urban areas, but has been used to assess urban SW and LW radiation and albedo (Chrysoulakis et al. 2018; Landier et al. 2018), variations in urban surface temperatures (Morrison et al. 2020, 2021), and mean radiant temperature (Dissegna et al. 2021), and to assess simpler radiative transfer models (e.g., SPARTACUS-Urban, Stretton et al. (2022)).

Formatted: Font color: Text 1

Formatted: Font color: Text 1

Formatted: Font color: Text 1

Formatted: Font color: Text 1

2.3 Single-layer street canyon approach (Harman)

~~The Harman et al. (2004) approach has a system of linear equations that compute the exact radiative transfer with vertically constant wall temperatures. Hogan (2019b) compared SPARTACUS-Urban to Harman et al.'s (2004) LW radiation after modifying Harman's horizontal geometry to have an exponential distribution, as assumed by SPARTACUS, but with all buildings having equal height. Agreement was found between the two models for the net outward LW flux from the ground and walls when greater than 4 streams were used by SPARTACUS Here, we use the Harman implementation in the SPARTACUS-Surface software package (implemented as in Sect. 4.2 of Hogan (2019)).~~

~~Harman assumes two parallel buildings of infinite length with constant height, *H*, separated by a constant street width, *W*. For this comparison, the total area of the ground, walls, and roofs are equal to the real-world domain (Sect. 3.1) with *H* set equal to the mean building height,~~ ~~$\overline{H}$~~~~, and the building fraction equal to the surface (~~~~$\lambda_p(z=0)$~~~~) value. The *H/W* is calculated using (Hertwig et al. (2020) their Eq. 3):~~

Harman et al. (2004) use a system of linear equations to compute the exact LW radiative transfer from one temperature per facet (e.g., one for walls). Hogan (2019b), after modifying Harman's horizontal geometry to have an exponential distribution, to be consistent with SPARTACUS's assumptions, finds agreement between the two models for the net outward LW flux from the ground and walls when SPARTACUS uses more than 4 streams. Here, the SPARTACUS-Surface software package (see Sect. 4.2 of (Hogan 2019a)) implementation of Harman is used for the simulations.

Harman assumes two parallel buildings of infinite length with constant height (*H*) separated by a constant street width (*W*). For this comparison, the real-world domain (Sect. 3.1) total area of the ground, walls, and roofs (i.e., building fraction at the surface ($\lambda_p(z = 0)$), and mean building height ($\overline{H} = H$) are used. *H/W* is calculated using (Hertwig et al. (2020), their Eq. 3):

$$\frac{H}{W} = \frac{\pi}{2}\frac{\lambda_f}{\left(1 - \lambda_p\right)} \tag{1}$$

where the frontal area index~~,~~ (λ_f) is calculated ~~using $\lambda_w = \lambda_f \pi$, where λ_w is the~~ from the total normalised wall area~~, calculated~~ ($\lambda_w = \lambda_f \pi$) using from the vertical profile of normalised building edge length~~,~~ (L) derived the from vertical profile:

$$\lambda_W = \sum_i^n L_i \Delta z_i\,. \tag{2}$$

~~This implementation of~~All Harman ~~requires a single~~simulations have only one temperature (i.e., not a profile) ~~for each of the three urban facets.~~per facet (i.e., wall, roof, ground).

3 Methodology

3.1 Model Domain

~~Our~~The evaluation ~~focuses on~~ is undertaken for a 2 km ~~x~~× 2 km area ~~of~~in central London, with residential and commercial buildings of varying horizontal extent and height (Figure 1a). ~~This domain's buildings have varying horizontal size and height, with some high-rise buildings used for residential and commercial purposes. The digital surface model (~~The DSM~~)~~ and digital elevation model (DEM)~~ used~~ are derived from "Virtual London" building footprint dataset (Evans et al. 2006). ~~For heights, the 25^{th} percentile of the DEM and 75^{th} percentile of the DSM are used giving individual buildings a single height, flat roofs, and flat, vertical walls.~~

~~For SPARTACUS-Urban, the required vertical profiles of λ_p and L are derived from a 1 m x 1 m building footprint raster, as rasterization removes internal walls between buildings. For DART, the 3D building roof and ground level geometry are determined from the DSM and DEM. The Stretton et al. (2022)~~To simplify buildings so they have flat both roofs and walls, for each building the 25^{th} percentile of the DEM and 75^{th} percentile of the DSM heights are used. For DART, the resulting 3D building roof DSM and ground DEM are used. The Stretton et al. (2022) 3D building model is improved slightly (e.g. shift in vertical plane, removal of some internal walls). The DART voxel resolution used ~~in DART~~ is 1 m vertically and 5.206 m horizontally. For SPARTACUS-Urban ~~has~~ the same vertical resolution as DART (1 m) is used. To remove internal walls between buildings, the SPARTACUS-Urban vertical profiles of λ_p and L are derived from a 1 m × 1 m building footprint raster.

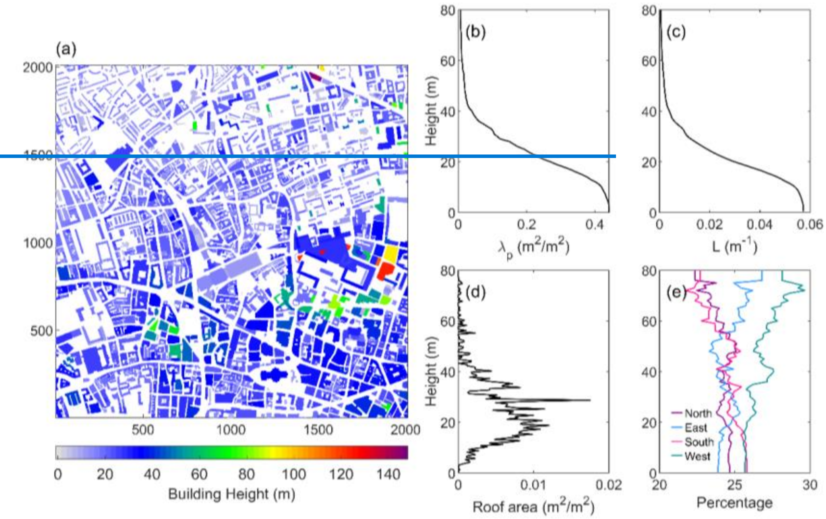

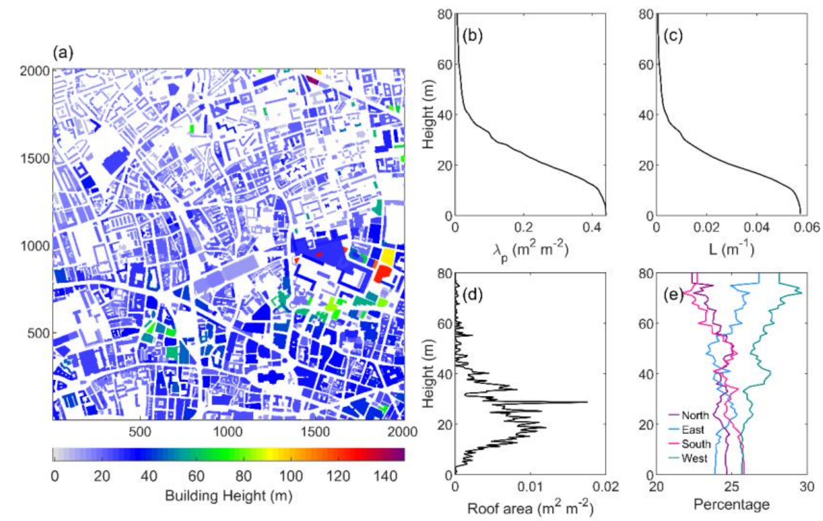

Figure 1: Low level of detail central London domain (i.e., flat roofs): (**a**) building heights, (**b**) building plan area fraction (λ_p) with height, (**c**) normalised building edge length (L) with height (Eq. 2), (**d**) roof area with height, (**e**) wall orientation distributions calculated from surface-classified DART emission output.

3.2 Observations used for radiative transfer inputs

In the model domain, three observation sites are present (Table 1). We focus on a day (27th August 2017) with detailed surface temperature observations and almost clear skies (< 45-min cloud mid-afternoon) (Morrison et al. 2020).

Given computational constraints, DART is run for a single wavelength (10 µm). Hence, we are unableWe choose 10 µm, as it is approximately central to use the LW infrared band, hence some additional uncertainty arises in SPARTACUS-Urban results for other wavelengths and broadband longwave flux measurements. cannot be used. Instead, we have rerun the ECMWF atmospheric radiation scheme using pressure, temperature and humidity profiles for the site 0.25° grid-cell from ERA5 (Hersbach et al. 2020) for that day (Figure 2), and extractedextract bottom-of-atmosphere (BOA) clear-sky downwelling spectral flux at 10 µm. For the SPARTACUS-Urban and Harman et al. (2004) simulations, changes were made to SPARTACUS-Surface so that emission is calculated for a single spectral wavelength. SPARTACUS-Surface additionally requires T_{Air}, but as we simulate radiative fluxes in a vacuum, this is set to 0 K. Each model requires an emissivity, ε, for each surface. We use a homogenous $\varepsilon = 0.93$, based on the mean urban value determinedFor the SPARTACUS-Urban and Harman et al. (2004) simulations, SPARTACUS-Surface is modified to calculate the single spectral wavelength emission.

Formatted: Font: Not Bold
Formatted: Font: Not Bold
Formatted: Font: Not Bold
Formatted: Font: Not Bold, Italic
Formatted: Font: Not Bold
Formatted: Font: Not Bold
Formatted: Font: Not Bold, Italic
Formatted: Font: Not Bold
Formatted: Font: Not Bold
Formatted: Font: Not Bold

SPARTACUS-Surface requires T_{Air}, but as we simulate radiative fluxes in a vacuum, it is set to 0 K. Each model requires an emissivity (ε) per surface. We assume homogenous value of 0.93, based on the mean urban value in the Kotthaus et al. (2014b) spectral library.

Facet surface temperatures are prescribed using thermal camera imagery (Optris PI-160 LW infrared cameras) observed for a 420 m x 420 m area within this domain (Morrison et al. 2020, 2021) (Figure 3). Detailed modelling has categorised these observations by facet type, sunlit/shaded, and orientation (Morrison et al. 2020, 2021). Surface temperatures are split into roof, ground, and cardinal wall orientation (*etc.*) types. Although we evaluate SPARTACUS-Urban across the whole day, to demonstrate the performance for multiple surface temperature configurations, we select times with distinct temperature profiles (e.g., just after sunrise, with no facet temperature range) and summarise the general model performance. As surface temperature processing constraints (Morrison et al. 2020) gives observations from 5:45 UTC (sunrise: 5:04 UTC), the models are runs for every hour from then to end of the day. The mid-afternoon cloud period is discarded, as no sunlit/shaded temperature range is observed (Figure 3).

Table 1: Sensors used from within domain (Figure 1a). Meteorological time series, and further details of observations within this domain can be found in Morrison et al. (2021)

Facet surface temperatures are prescribed using thermal camera imagery (Optris PI-160 LW infrared cameras) observed for a 420 m × 420 m area within this domain (Morrison et al. 2020, 2021) (Figure 3). Detailed modelling has categorised these observations by facet type, sunlit/shaded, and orientation (Morrison et al. 2020, 2021). Surface temperatures are split into roof, ground, and cardinal wall orientation (*etc.*) types. Although we evaluate SPARTACUS-Urban across the whole day, to demonstrate the performance for multiple surface temperature configurations, we select times with distinct temperature profiles (e.g., just after sunrise, with no facet temperature range) and summarise the general model performance. As surface temperature processing constraints (Morrison et al. 2020) gives observations from 5:45 UTC (sunrise: 5:04 UTC), the models are runs for every hour from then to end of the day. The mid-afternoon cloud period is discarded, as no sunlit/shaded temperature range is observed (Figure 3).

Table 1: Sensors used from within domain (Figure 1a). Meteorological time series, and further details of observations within this domain can be found in Morrison et al. (2021)

Site	Full name	Latitude °N	Longitude °W	Instruments
BCT	Barbican Cromwell Tower	51.5206	0.09230	Davis weather station
IMU	Islington Michael Cliffe House Upper	51.526	0.1061	Davis weather station Kipp and Zonen CNR1 radiometer Optris Pi160 infrared thermal camera
WCT	Wycliffe Court Tower	51.5267	0.1036	Optris Pi160 infrared thermal camera

Formatted Table

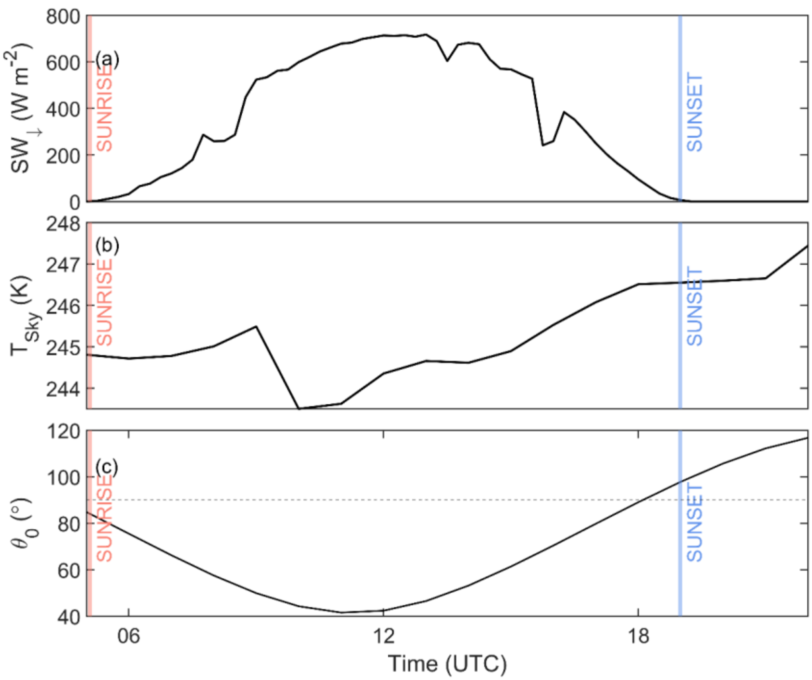

Figure 2: Diurnal timeseries for 27th August 2017 of (**a**) downwelling shortwave ($SW_{\downarrow}$) observations from a Kipp and Zonen CNR1 radiometer located at IMU, (**b**) ~~Clear~~clear-sky 10-~~mm~~μm brightness temperatures calculated from ERA5, and (**c**) solar zenith angle (θ_0). Additional meteorological observations for the day of interest are shown in Morrison et al. (2021).

Formatted: Font: Not Bold
Formatted: Font: Not Bold
Formatted: Font: Not Bold
Formatted: Font: Not Bold, Subscript
Formatted: Font: Not Bold
Formatted: Font: Not Bold
Formatted: Font: Not Bold
Formatted: Font: Not Bold
Formatted: Font: Not Bold
Formatted: Font: Not Bold
Formatted: Font: Not Bold

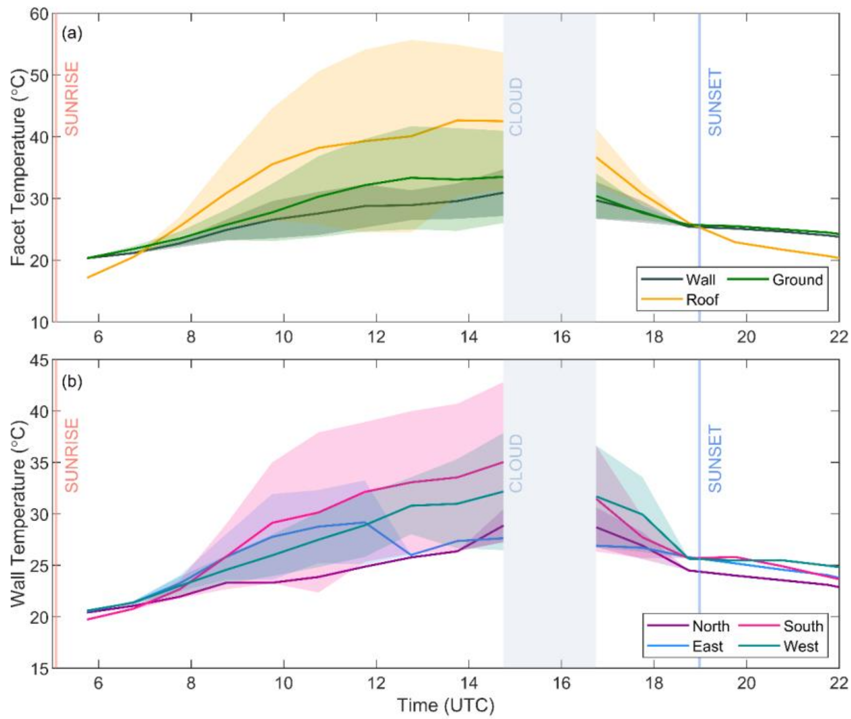

Figure 3: ~~**Mean**~~ Observed mean (line) and range (shading~~**; mean [**~~, [between sunlit to shaded areas]) temperature ~~**observations**~~on 27[th] August 2017 (Morrison et al. 2021) for each (**a**) facet type (walls – all weighted equally) and (**b**) wall azimuthal orientation.

3.3 Model surface temperature (*T*) prescription

The three radiative transfer models (Sect. 2) require different T inputs. To assess the sources of error between SPARTACUS-Urban and DART (i.e., radiation calculation or surface temperature values), two complexities of model runs are undertaken. First, simulations assume an isothermal temperature within each surface type, with DART surfaces prescribed the single mean T from the camera observations (Figure 3a, line). To match this, SPARTACUS-Urban roofs and ground are prescribed the mean DART input temperature. For SPARTACUS-Urban T_{Wall}, each wall orientation is weighted equally (Figure SM 1), following the SPARTACUS-Urban assumption that walls equally face in all directions, such that:

$$T_{Wall} = (T_{Wall\,N} + T_{Wall\,E} + T_{Wall\,S} + T_{Wall\,W})/4 \quad (3)$$

where $T_{,Wall\ N\text{-}E\text{-}S\text{-}W}$ are one of the four cardinal directions. For Harman, the same temperatures as SPARTACUS-Urban are

Formatted: Font: Not Bold
Formatted: Font: Not Bold
Formatted: Font: Not Bold
Formatted: Font: Not Bold
Formatted: Font: Not Bold
Formatted: Font: Not Bold
Formatted: Font: Not Bold
Formatted: Font: Not Bold
Formatted: Font: Not Bold

used.

Non-isothermal surface temperatures varying by sunlit – shaded status allow for horizontal and vertically differences by facet type. These can be represented in multi-layer energy exchange schemes. DART scenes can have a A temperature mean and range (Fig. 3)can be prescribed across a in DART allowing sunlit-shaded variations. However, given level of detail of the surface type (e.g., roof, west facing wall, east facing wall). This allows for the impacts of variation in SW flux to be simulated. A model used (Figure 1) the observed surface temperatures are not directly usable as camera pixels has much higher resolution than the DART SW simulation istriangles. DART SW simulations are used to determine whether aeach facet triangle is sunlit or in shadeshaded, and therefore which temperature to utilize. (maximum/minimum) range (Figure 3) is assigned by type (e.g., roof, west facing wall, east facing wall). As noted, as DART triangles may have whole wall resolution but only one prescribed temperature.

To enable SPARTACUS-UrbanAs it is complex to captureextract the horizontal surface vertical profile of temperature variations,for each surface type from DART, solar zenith angle (θ_0) dependent SW SPARTACUS-Urban simulations are conductedused to estimate the sunlit fraction of sunlitfor the walls or roofs at each height interval ($F_{Sun,Wall,i}$,) and roofs $F_{Sun,Roof,i}$,) by height interval, and for the ground ($F_{Sun,Ground}$), using the solar zenith angle (θ_0), with). The shaded fractions determinedare obtained by the difference e.g., $F_{Sh,Wall,i}$ ($F_{Sh,Wall,i} = 1 - F_{Sun,Wall,i}$). The appropriate DART sunlit and (shaded) temperatures are assigned to SPARTACUS-Urbans sunlit (shaded) fraction. Similarly, the sunlit and shaded roof temperatures ($T_{Sun,Roof}$, $T_{Sh,Roof}$) are simply weighted at each height by the appropriate sunlit and shaded fractions to obtain $T_{Roof,i}$. The and at z=0 for the ground temperatures ($T_{Ground,sun}$, $T_{Ground,sh}$) are treated in the same way, but at just $z=0$). Thus, enabling SPARTACUS-Urban to capture the horizontal surface temperature variations.

As the four wall orientations have different temperatures depending on their shadow history (Morrison et al. 2021), for SPARTACUS-Urban we weight them to obtain one average sunlit and shaded wall temperature ($T_{Wall,sun}$, $T_{Wall,sh}$). Given the SPARTACUS-Urban assumption that walls face equally in all directions, we weight the sunlit and shaded temperatures (as Eq. 3), but use the solar azimuth angle, (Ω,) to determine the 'dominant' sunlit wall orientation. The dominant sunlit facing surface (e.g., south) temperature (in this example, $T_{Sun,South}$) is double weighted in Eq. 3 (i.e., replacing $T_{Sun,North}$) assuming the wall 180° (i.e., north facing surfaces in example) are shaded. The opposite is done for the $T_{Sh,Wall}$, obtaining (for this example):

$$T_{Sun,Wall} = 0.0 \cdot T_{Sun,Wall\,N} + 0.25 \cdot T_{Sun,Wall\,E} + 0.25 \cdot T_{Sun,Wall\,W} + 0.5 \cdot T_{Sun,Wall\,S}, \quad (4)$$

$$T_{Sh,Wall} = 0.5 \cdot T_{Sh,Wall\,N} + 0.25 \cdot T_{Sh,Wall\,E} + 0.25 \cdot T_{Sh,Wall\,W} + 0.0 \cdot T_{Sh,Wall\,S}. \quad (5)$$

The $T_{Wall,sh}$ and $T_{Wall,sun}$ are weighted using $F_{Sun,Wall,i}$ and $F_{Sh,Wall,i}$ to determine the $T_{Wall,i}$ for each height:

$$T_{Wall,i} = F_{Wall,sun,i} T_{Wall,sun} + F_{Wall,sh,i} T_{Wall,sh}. \quad (6)$$

Formatted: English (United Kingdom)

Formatted: English (United Kingdom)

Formatted: English (United Kingdom)

To visualise this at several times see Figure SM 1. Combining $F_{Sun,Wall,i}$ and $F_{Sun,Roof,i}$ gives a larger weight to warmer sunlit surface temperatures in the simulations, better matching the emission from the DART model scenes.

~~For the Harman et al. (2004)~~

For the Harman et al. (2004) simulations, area-weighted surface temperatures from the SPARTACUS-Urban profiles are used:

$$T_{Wall} = \sum_{i}^{n} T_{Wall,i}\left(\lambda_{Wall,i}/\lambda_{Wall}\right) \tag{7}$$

where $\lambda_{Wall,i}$ is the exposed normalised wall area at each height, which is normalised by the total wall area, λ_W. Eq. 7 is also applied to roofs. This ensures that warmer surfaces at the top of the canopy with small areas are not overweighted.

3.4 Evaluation Metrics

We evaluate SPARTACUS-Urban using DART by comparing the profiles of LW upwelling and downwelling clear-air spectral fluxes ($LW_\uparrow$, $LW_\downarrow$), and the intercepted, outgoing, and net (= incoming – outgoing, relevant for facet temperature evolution) flux into walls, roofs, and ground (i.e., $LW_{In,Wall}$, $LW_{Out,Wall}$, LW^*_{Wall}). The LW clear-air fluxes have units of W m^{-2} μm^{-1} of the entire horizontal scene, while the fluxes from walls and roofs have units W m^{-3} μm^{-1}, as we divide by the layer thickness (1 m) to obtain a resolution independent flux.

For the comparison between SPARTACUS-Urban and DART, we examine the downwelling longwave at the base of the canopy, and the upwelling longwave at the top of the canopy in DART (H_{max}) to obtain a normalised bias error. The $LW_\uparrow$ flux profiles are evaluated using the normalized bias error at a specified height (*nBE*), expressed as a percentage of the DART flux:

$$nBE = \frac{LW_{SU} - LW_{\mathrm{DART}}}{LW_{\mathrm{DART}}} 100\%. \tag{8}$$

We compare the differences in the wall and roof fluxes between the two models by using a nBE in the total interception, emission, and net LW flux, calculated from 1 m to H_{max}.

4 Results

4.1 Prescribed surface temperatures

The $F_{Sun,Wall,i}$ and $F_{Sun,Roof,i}$ are calculated from SPARTACUS-Urban SW simulations for each time period (Figure 4). The sunlit fraction into the canopy increases as zenith angle, θ_0, decreases until about 11:45 UTC (Figure 2). As more walls become illuminated within the canopy, there is an increase in T_{Wall} (Figure 3, Figure 4). As θ_0 increases again (Figure 2c), the within-canopy surfaces become more shaded than sunlit.

From combining the F_{Sh} and F_{Sun} profiles with the DART prescribed facet T (Eq. 4 ~~to~~ –6) the T_{Wall} and T_{Roof} profiles are obtained (Figure 5). At 5:45 UTC all DART temperatures are the same, so all temperature configurations and SPARTACUS-Urban temperatures are equal. At 7:45 UTC, the first vertical variations in temperature occur with sunlit roof facets higher in the canopy causing warmer temperatures above. Both 11:45 UTC and 13:45 UTC share similar T_{Wall} profiles, and do not have much influence from the warmer south facing walls despite their greater weighting. The most different T_{Roof} profile, spanning the widest temperature range, occurs at 17:45 UTC.

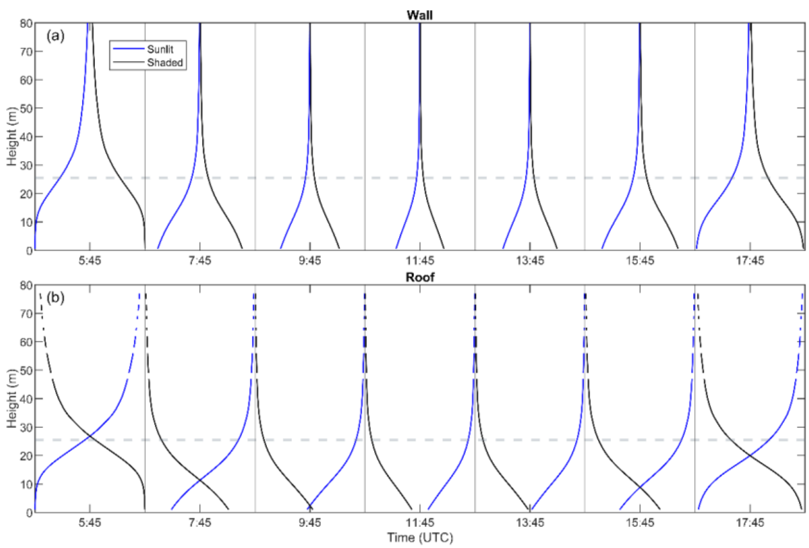

Figure 4: Sunlit (blue) and shaded (black) fraction of (**a**) walls and (**b**) roofs during the study day from SPARTACUS-Urban shortwave simulations using solar zenith angles (~~**Figure 2).**~~Figure 2). Lines are shown as dashed when no roofs occurs at a height. Mean building height ($\bar{H}$= 25.5 m, grey dashed).

Formatted: Font: Not Bold

Formatted: Font: Not Bold

Formatted: Font: Not Bold

Formatted: Font: Not Bold

Formatted: Font: Not Bold

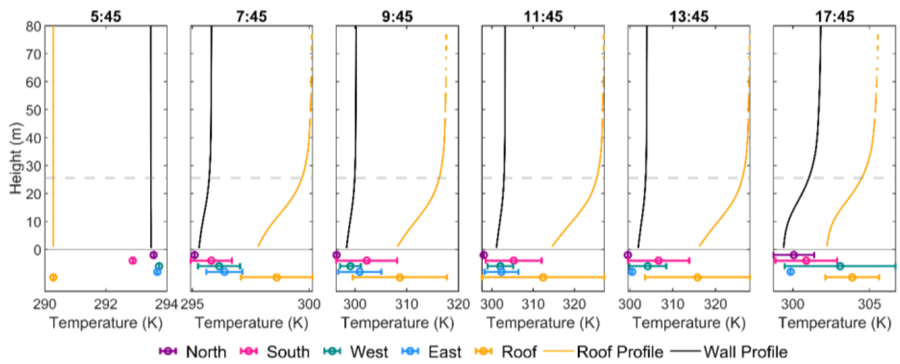

Figure 5: Temperature profiles at six times (UTC) used in SPARTACUS-Urban simulations (averaging methods, Sect. 3.33.3) with temperatures prescribed to DART surface types given in the error bars below each set of temperature profiles, with the mean temperature denoted by open circles, and sunlit-shaded range given (**Figure 3).**Figure 3), Note x-axes differ between panels.

Formatted: Font: Not Bold

Formatted: Font: Not Bold

Formatted: Font: Not Bold

4.2 Comparison of SPARTACUS-Urban and DART: One facet temperature (*T*)

First, when *T* does not varyhave sunlit-shaded variations, there is good agreement between SPARTACUS-Urban and DART. There is good agreement for both $LW_{\uparrow}$ at the top of the canopy (nBE < 0.5% across the whole day, Table 2, Figure SM 3 toFigure 6, Figure SM 3 - 7) (Figure 6),), and for the $LW_{\downarrow}$ across the day (nBE ~2%). The $LW_{Out,Wall}$ nBE is < 0.1%, and the nBE for LW^*_{Wall} is 8-11%. The nBE is less when T_{Wall} is warmer (i.e., middle of day). The larger error in LW^*_{Wall} is caused by a small net flux as $LW_{In,Wall}$ and $LW_{Out,Wall}$ cancel each other thus small errors result in large nBE.

Field Code Changed

SPARTACUS-Urban slightly underestimates $LW_{In,Wall}$ and $LW_{Out,Wall}$ (Figure 6) at the base of the canopy, therefore LW^*_{Wall} is slightly overestimated. SPARTACUS-Urban overestimates $LW_{In,Roof}$ below $\overline{H}$. With just one T_{Roof} per time interval, $LW_{Out,Roof}$ error is small (nBE ~3%), causing underestimates of LW^*_{Roof} and larger nBE (5.5 to 8.5 %).

Across the multiple cases for different facet *T* and with different differences inbetween facet *T* (e.g., magnitude of $T_{Roof} > T_{Wall}$), the agreement is consistent between the two models. These differences may have arisen due to the geometry assumptions in SPARTACUS-Urban or the wall temperature averaging, but despite this, their magnitudes remain low.

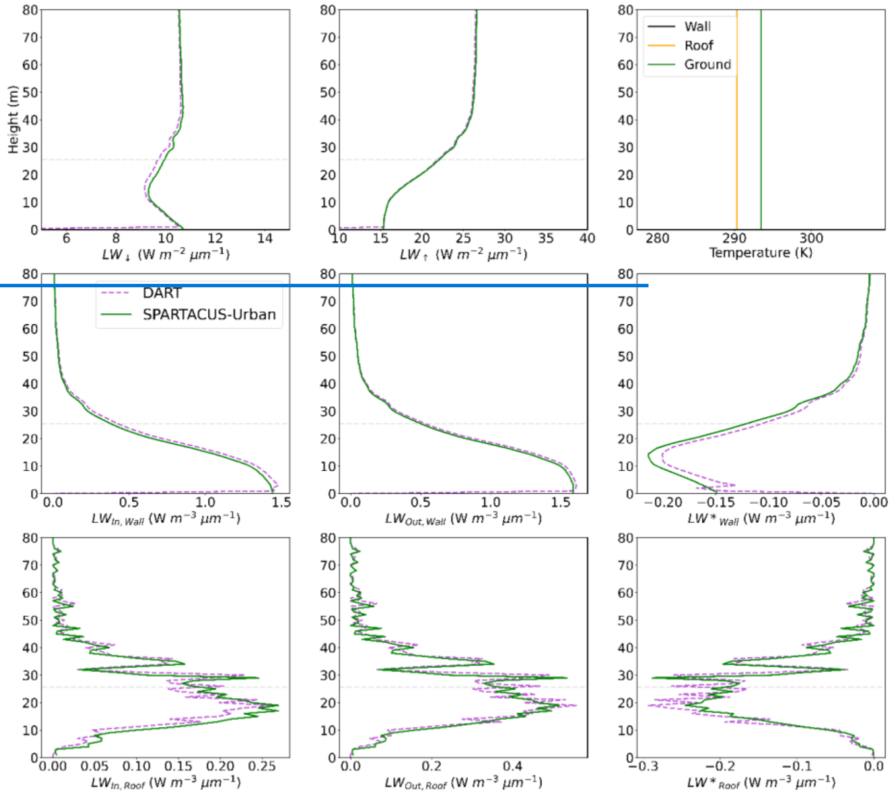

Height (m)
LW↓ (W m⁻² μm⁻¹)
LW↑ (W m⁻² μm⁻¹)
Wall
Roof
Ground
Temperature (K)
DART
SPARTACUS-Urban
LW In, Wall (W m⁻³ μm⁻¹)
LW Out, Wall (W m⁻³ μm⁻¹)
LW* Wall (W m⁻³ μm⁻¹)
LW In, Roof (W m⁻³ μm⁻¹)
LW Out, Roof (W m⁻³ μm⁻¹)
LW* Roof (W m⁻³ μm⁻¹)

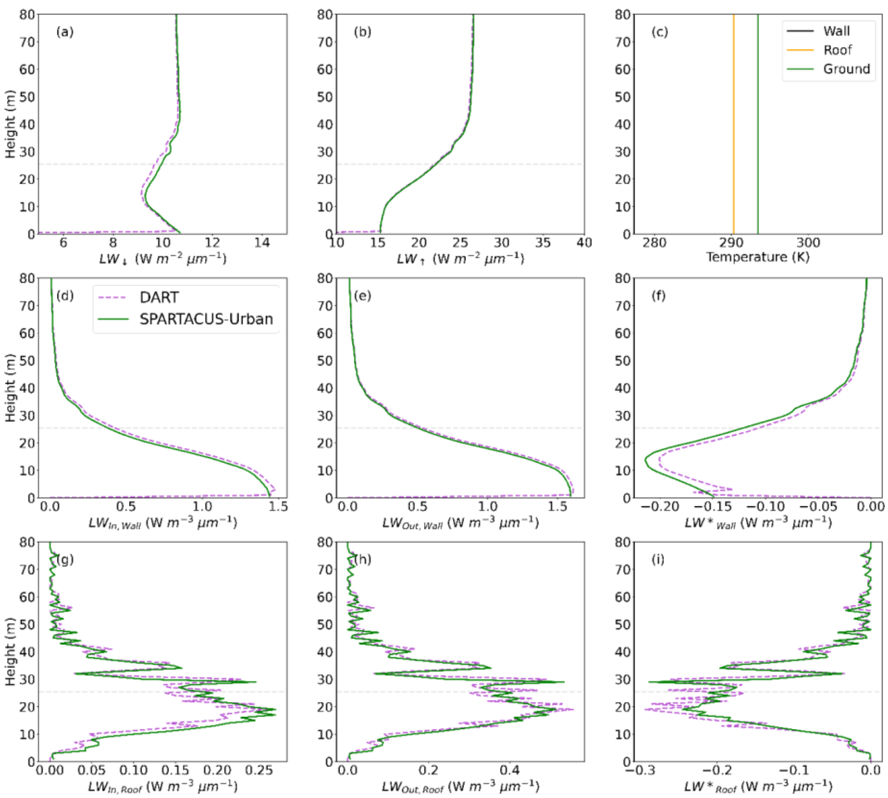

Figure 6: Longwave fluxes (LW) for a 2 km ~~x 2km~~ × 2 km domain in central London (Figure 1) simulated with SPARTACUS-Urban (green) and DART (purple) with an emissivity of 0.93 at 5:45 UTC on the 27th August 2017 with (c) single facet T: (**a**) downwelling clear air flux ($LW_{\downarrow}$), (**b**) upwelling clear air flux ($LW_{\uparrow}$), (~~c,~~ **d**~~, e-~~f) wall interception, outgoing and net flux ($LW_{In,Wall}$, $LW_{Out,Wall}$, LW^*_{Wall}), (~~f,~~ **g**~~, h-~~ i) roof interception, outgoing and net flux ($LW_{In,Roof}$, $LW_{Out,Roof}$, LW^*_{Roof}). Prescribed facet temperatures using: a single temperature per surface type for DART, and (**c**) single temperatures per facet type for SPARTACUS-Urban.

Table 2: Evaluation of SPARTACUS-Urban (cf. DART) for a 2 km × 2 km domain in central London on an August day, for facets prescribed a single surface temperature. Upwelling and downwelling clear-air fluxes ($LW_{\downarrow}$, $LW_{\uparrow}$), and the total outgoing and net flux into each urban facet (wall, roof, ground, e.g., $LW_{Out,Wall}$, LW^*_{Wall}), assessed using the normalised bias error (nBE, Eq. 8).

Time	$LW_{\downarrow}$, z = 1		$LW_{\uparrow}$, $z = H_{max}$		LW^*_{Wall}	LW^*_{Roof}	LW^*_{Ground}	$LW_{Out,Wall}$	$LW_{Out,Roof}$	$LW_{Out,Ground}$
(UTC)	DART	nBE (%)	DART	nBE (%)	nBE (%)	nBE (%)	nBE (%)	nBE (%)	nBE (%)	nBE (%)
5:45	10.5	2.2	26.6	0.47	11	-8.2	-3.3	0.047	-3.3	-0.24
7:45	10.9	2.2	28.9	0.19	9.8	-6.9	-3.1	0.023	-3.1	-0.24
9:45	11.3	2.3	32.0	-0.099	8.5	-6.0	-2.9	0.0073	-2.9	-0.24
11:45	11.6	2.4	33.7	-0.18	8.5	-5.8	-2.7	0.0052	-2.7	-0.24
13:45	11.8	2.4	34.7	-0.27	8.2	-5.5	-2.7	-0.0043	-2.7	-0.24

Formatted: Font: Not Bold
Formatted: Font: Not Bold
Formatted: Font: Not Bold
Formatted: Font: Not Bold
Formatted: Font: Not Bold
Formatted: Font: Not Bold
Formatted: Font: Not Bold
Formatted: Font: Not Bold
Formatted: Font: Not Bold, Font color: Text 1
Formatted: Font: Times New Roman, Not Bold, Font color: Text 1
Formatted: Font: Not Bold, Font color: Text 1
Formatted: Font: Times New Roman, Not Bold, Font color: Text 1
Formatted: Font: Not Bold, Font color: Text 1
Formatted: Font color: Text 1
Formatted: Font: Not Bold, Font color: Text 1
Formatted: Font: Times New Roman, Not Bold, Font color: Text 1
Formatted: Font: Not Bold, Font color: Text 1
Formatted: Font: Times New Roman, Not Bold, Font color: Text 1
Formatted: Font: Not Bold, Font color: Text 1
Formatted: Font: Not Bold
Formatted: Font: Not Bold
Formatted: Font: Not Bold

17:45	11.6	2.4	31.2	0.20	9.9	-6.9	-3.3	0.029	-3.3	-0.23
19:45	11.3	2.2	29.1	0.40	11	-7.9	-3.1	0.047	-3.1	-0.24
21:45	11.2	2.2	28.4	0.45	11	-8.2	-3.2	0.047	-3.2	-0.24

4.3 Comparison of SPARTACUS-Urban and DART: Varying facet temperature with -solar irradiance

Second,- we compare the two models when facets are prescribed a T range. Here, SPARTACUS-Urban has good agreement with DART for $LW_{\downarrow}$ at the base of the canopy (nBE 1.7- 2.9%),%, Table 3), and at the top of the canopy, for all times (Table 2, Figure 7, Figure 8,- 8, Figure SM 8 to Figure SM- 12). There are some disagreements towards the centre of the canopy, ~ (~10 – 40 m,), at all times, where SPARTACUS-Urban overestimates the $LW_{\downarrow}$. There is also good agreement in $LW_{\uparrow}$ up to ~40 m. SPARTACUS-Urban has good agreement (nBE < 0.5%) at the start and end of the day when there is a small range in facet T (Figure 5), and so temperature averaging (i.e., wall orientation) has little impact. The nBE in $LW_{\uparrow}$ is poorest in middle of the day (11:45 UTC – 14:45 UTC) when the facets have a large range in temperature but is still < 2.5 %.

The largest errors occur in the LW roof fluxes. The $LW_{In,Roof}$ is always overestimated by SPARTACUS-Urban overestimates all the $LW_{In,Roof}$ below the $\overline{H}$ (as in Sect. 4.2). However, $LW_{Out,Roof}$ is similar tobetween SPARTACUS-Urban and DART (nBE ~ 3%), suggesting the $T_{Sun,Roof}$ and $T_{Sh,Roof}$ averaging method provides a good approximation to DART. TheHence, SPARTACUS-Urban underestimates the LW^*_{Roof} is underestimated in SPARTACUS-Urban below the $\overline{H}$, with nBE 6 – 8 %. These differences couldmay be associated with SPARTACUS-Urban building height havingthe 1 m vertical resolution whereasused in SPARTACUS-Urban cf. DART's roof fluxes arebeing aggregated to each voxel top. Despite this, the vertical profiles of LW_{Roof} fluxes in SPARTACUS-Urban and DART are still close (Figure 7d, h, lg-i).

The SPARTACUS-Urban LW wall fluxes generally compare well to DART. There are slight differences in the $LW_{In,Wall}$ close to the surface, which is likely associated with is attributable to removal of the internal building walls being removed (Sect. 3.1). The nBE in $LW_{Out,Wall}$ is ~8% throughout the day, for For all surface temperature configurations. The nBE in, the $LW_{Out,Wall}$ the nBE is ~8% throughout the day. Through the day LW^*_{Wall} nBE varies from 0 – 10% through the day, with it%. It is smallest (11:45 UTC – 14:45 UTC) when there is the largest T_{Wall} variation (is largest (11:45 – 14:45 UTC, Figure 3). The good agreement in $LW_{Out,Ground,}$ suggests the averaging method for sunlit and shaded temperatures performs well. SPARTACUS-Urban underestimates LW^*_{Ground} but with low nBE (2 - 5 %).

Formatted: Font: Times New Roman

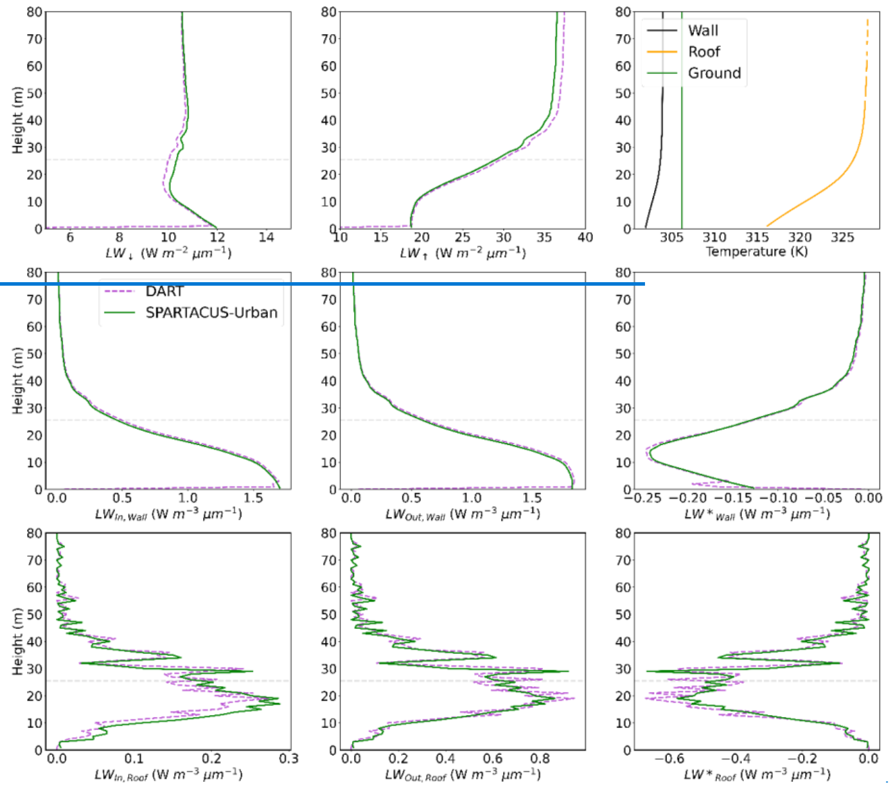
Height (m)
LW↓ (W m⁻² μm⁻¹)
LW↑ (W m⁻² μm⁻¹)
Wall
Roof
Ground
Temperature (K)
DART
SPARTACUS-Urban
$LW_{In,Wall}$ (W m^{-3} μm^{-1})
$LW_{Out,Wall}$ (W m^{-3} μm^{-1})
$LW*_{Wall}$ (W m^{-3} μm^{-1})
$LW_{In,Roof}$ (W m^{-3} μm^{-1})
$LW_{Out,Roof}$ (W m^{-3} μm^{-1})
$LW*_{Roof}$ (W m^{-3} μm^{-1})

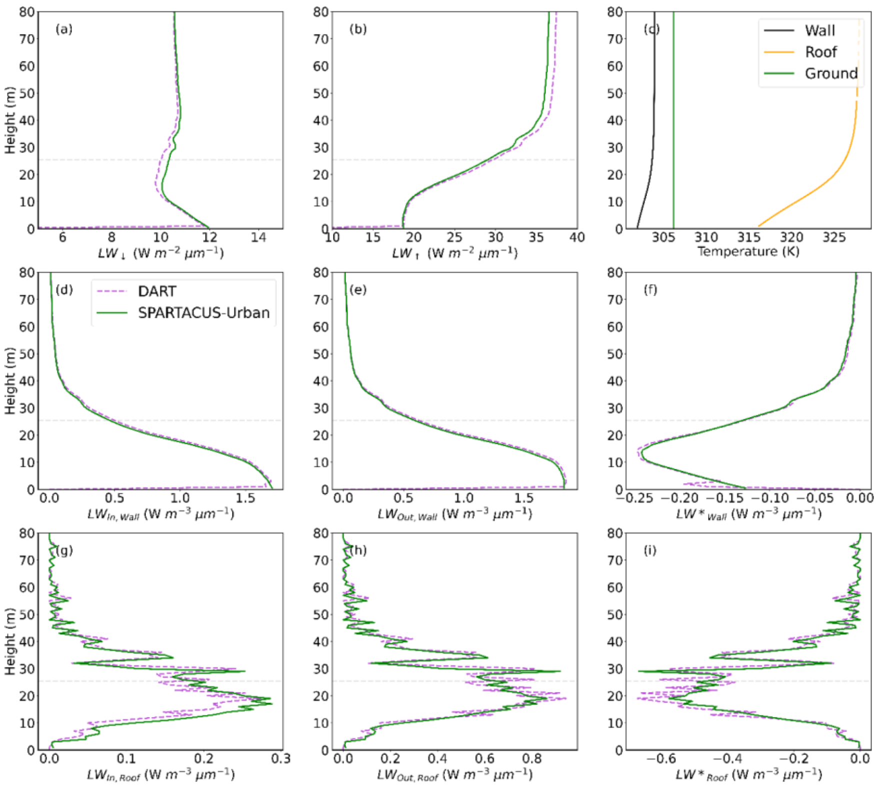

Figure 7: As Figure 6, but for facet temperatures prescribed based on SW simulations at 13:45 UTC. DART simulations use a full temperature profile.

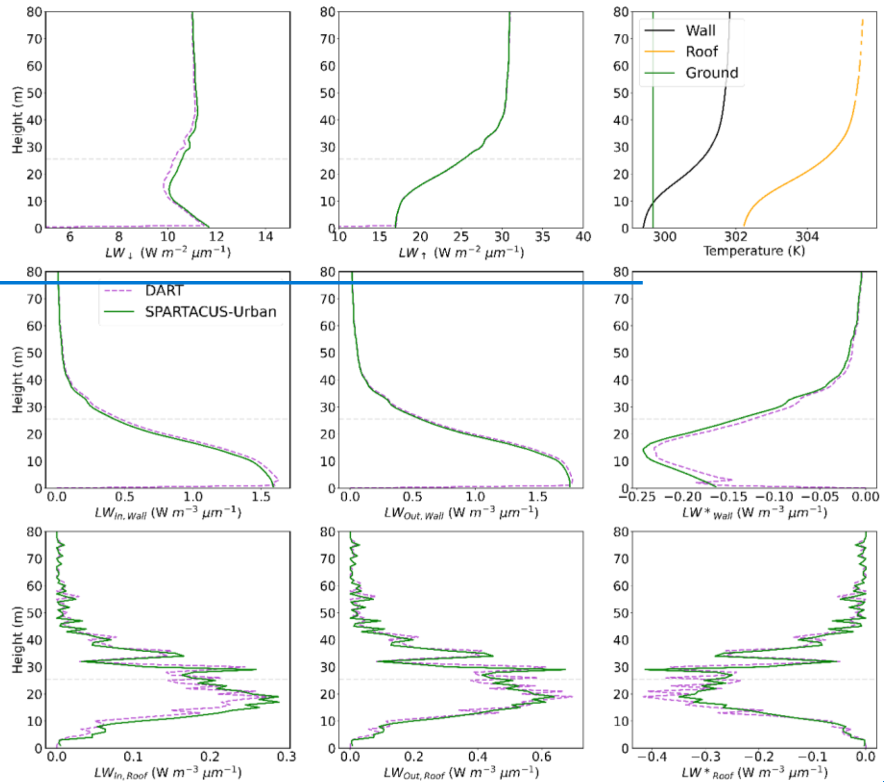

: Longwave fluxes (LW) for a 2 km x 2km domain in central London (Figure 1) simulated with SPARTACUS-Urban (green) and DART (purple) with an emissivity of 0.93 at 13:45 UTC on the 27th August 2017: (**a**) downwelling clear air flux ($LW_{\downarrow}$), (**b**) upwelling clear air flux ($LW_{\uparrow}$), (**d-f**) wall interception, outgoing and net flux ($LW_{In,Wall}$, $LW_{Out,Wall}$, LW^{*}_{Wall}), (**g-i**) roof interception, outgoing and net flux ($LW_{In,Roof}$, $LW_{Out,Roof}$, LW^{*}_{Roof}). Prescribed facet temperatures based on SW simulations at 13:45 using: a full 3D temperature field for DART, and (**c**) temperature profiles per facet type for SPARTACUS-Urban.

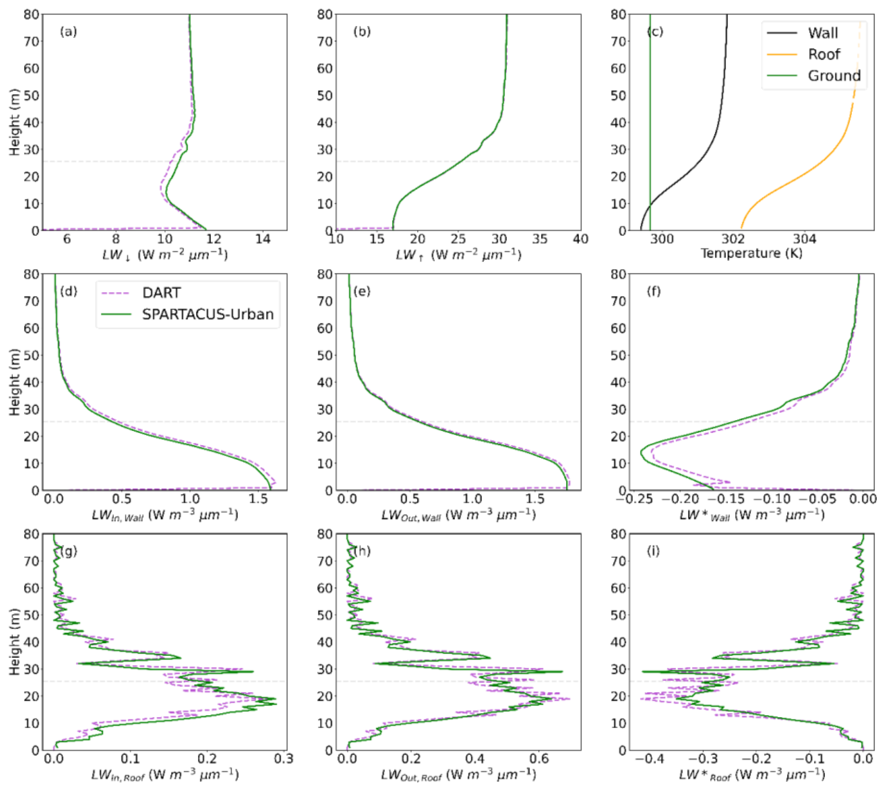

Figure 8~~: As Figure 7, but for 17:45 UTC~~

: Longwave fluxes (LW) for a 2 km × 2 km domain in central London (Figure 1) simulated with SPARTACUS-Urban (green) and DART (purple) with an emissivity of 0.93 at 17:45 UTC on the 27th August 2017: (**a**) downwelling clear air flux ($LW_{\downarrow}$), (**b**) upwelling clear air flux ($LW_{\uparrow}$), (**d-f**) wall interception, outgoing and net flux ($LW_{In,Wall}$, $LW_{Out,Wall}$, LW^*_{Wall}), (**g-i**) roof interception, outgoing and net flux ($LW_{In,Roof}$, $LW_{Out,Roof}$, LW^*_{Roof}). Facet temperatures used are prescribed based on SW simulations at 17:45, with DART using a full 3D temperature field and (**c**) SPARTACUS-Urban using temperature profiles for each facet type.

Table 3~~: As Table 2, but facets T profile based on SW simulations. DART full temperature profile,~~

: Evaluation of SPARTACUS-Urban (cf. DART) for a domain in central London on an August day, for SPARTACUS-Urban facets prescribed a surface temperature profile based on SW simulations, and DART using a full temperature field. Upwelling and downwelling clear-air fluxes ($LW_{\downarrow}$, $LW_{\uparrow}$), and the total outgoing and net flux into each urban facet (wall, roof, ground, e.g., $LW_{Out,Wall}$, LW^*_{Wall}), assessed using the normalised bias error (nBE, Eq. 8).

Time	$LW_{\downarrow}$, z = 1		$LW_{\uparrow}$, z = H_{max}		LW^*_{Wall}	LW^*_{Roof}	LW^*_{Ground}	$LW_{Out,Wall}$	$LW_{Out,Roof}$	$LW_{Out,Ground}$
(UTC)	DART	*nBE* (%)	DART	nBE (%)	nBE (%)	nBE (%)	nBE (%)	nBE (%)	nBE (%)	nBE (%)
7:45	10.8	1.9	29.1	-0.31	8.0	-7.3	-3.3	0.047	-3.3	-0.23

Formatted Table

Formatted: Centered

9:45	11.3	1.7	33.9	-2.0	1.7	-7.3	-3.1	-0.38	-3.1	-0.42
11:45	11.6	2.7	37.2	-2.2	4.0	-6.6	-2.0	-1.6	-2.0	-0.28
12:45	11.7	2.2	37.9	-2.5	0.62	-6.8	-4.8	-1.5	-4.8	-0.923
13:45	11.8	2.3	37.6	-2.4	0.13	-6.9	-3.0	-1.7	-3.0	-0.48
14:45	11.8	2.9	37.3	-2.3	5.2	-7.7	-2.0	-1.7	-2.0	-0.032
17:45	11.5	2.4	31.2	-0.15	10	-7.8	-5.0	-2.0	-5.0	-0.70

Formatted: Centered

Formatted: Centered

Formatted: Centered

Formatted: Centered

Formatted: Centered

Formatted: Centered

4.4 Impact of surface temperature prescription inprescribed to SPARTACUS-Urban

Third, as As SPARTACUS-Urban performs well (cf. DART) for both temperature scenarios (Sect. 4.2 4.34.2, 4.3), we compareexamine differences between using a single facet temperatures (Sect. 4.2) or a profile ($T_{Profile}$, Sect. 4.3). To ensure the average emission is the same in each, the single temperature SPARTACUS-Urban simulations use weighted averagemean vertical profiles of T_{Wall} and T_{Roof} (as Eq. 7, as for Harman). This ensures the average emission is the same for each simulation, allowing both simulations to be compared.

There are negligible differences between the $LW_{\uparrow}$ and $LW_{\downarrow}$ within the canopy, for both simulations (Figure 9). As the geometry is identical between simulations, the $LW_{In,Roof}$ and $LW_{In,Wall}$ are also the same. The nBE in the $LW_{Out,Roof}$ and $LW_{Out,Wall}$ are small (<(< -0.2%), but larger in thefor $LW_{Out,Ground}$ (nBE < 4%) (Table 4, Figure SM 13). The largest nBE are in thefor LW^*_{Wall} (nBE < -3%) and LW^*_{Ground} (nBE < 4.8%). The $LW_{Out,Wall}$ switches from an overestimateover- to underestimate in the single T simulation at ~12 m, corresponding to where the single wall temperature overestimates,over- and then underestimates, the T profile. This then impacts the LW^*_{Wall} profile. These changes in wall and roof temperature profiles mimic the cumulative profiles in the wall and roof fraction (Figure SM 2).

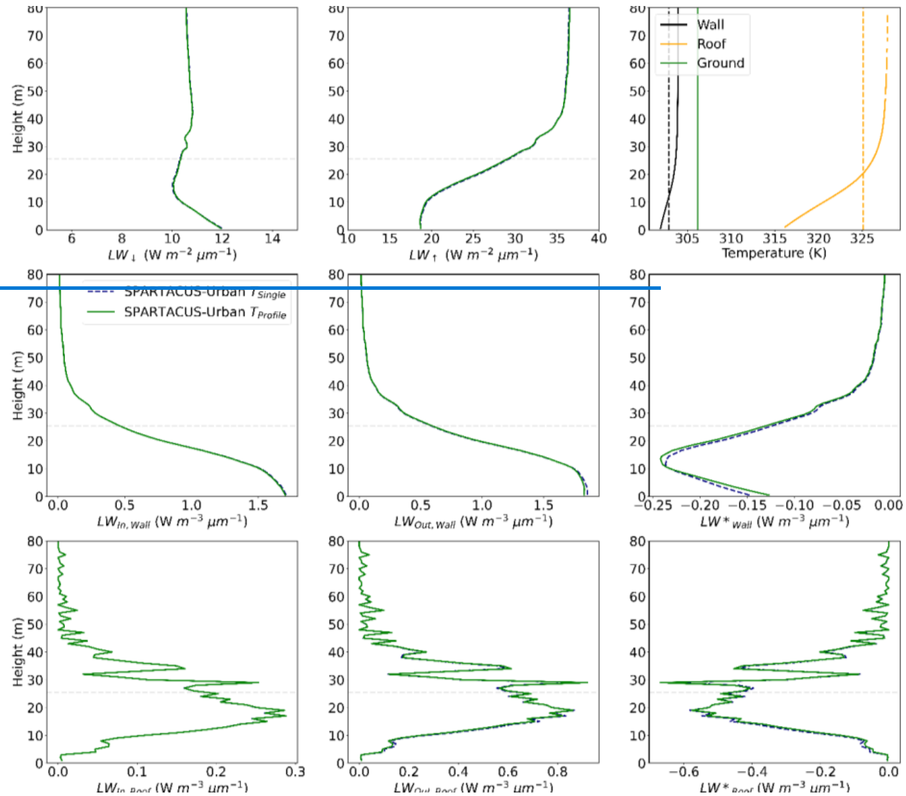
Height (m)
LW↓ (W m⁻² μm⁻¹)
LW↑ (W m⁻² μm⁻¹)
Wall
Roof
Ground
Temperature (K)
SPARTACUS-Urban T_Single
SPARTACUS-Urban T_Profile
LW_In,Wall (W m⁻³ μm⁻¹)
LW_Out,Wall (W m⁻³ μm⁻¹)
LW*_Wall (W m⁻³ μm⁻¹)
LW_In,Roof (W m⁻³ μm⁻¹)
LW_Out,Roof (W m⁻³ μm⁻¹)
LW*_Roof (W m⁻³ μm⁻¹)

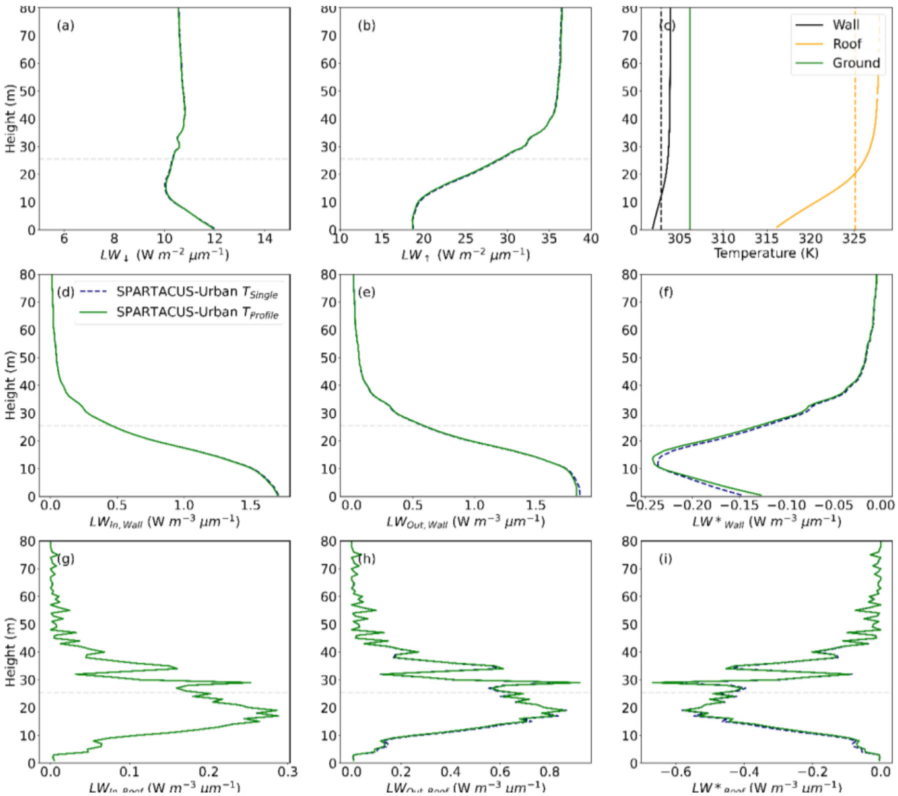

Figure 9: Longwave (LW) SPARTACUS-Urban simulations for a 2 km × 2 km domain in central London (Figure 1) with an emissivity of 0.93 for 13:45 UTC with on the 27th August 2017: (**a**) downwelling clear air flux ($LW_{\downarrow}$), (**b**) upwelling clear air flux ($LW_{\uparrow}$), (**d-f**) wall interception, outgoing and net flux ($LW_{In,Wall}$, $LW_{Out,Wall}$, LW^{*}_{Wall}), (**g-i**) roof interception, outgoing and net flux ($LW_{In,Roof}$, $LW_{Out,Roof}$, LW^{*}_{Roof}). Facet temperatures prescribed are (**c**) a single (*T*, *Single*) and range temperature per facet (T_{Single}, black dashed) and using temperature profiles for each facet type ($T_{Profile}$) facet *T*, , green)

Formatted: Font: Not Bold

Formatted: Font: Not Bold

Formatted: Font: Not Bold, Font color: Text 1

Formatted: Font: Not Bold, Font color: Text 1

Table 4: **As Table 2, but**Comparison between **two** SPARTACUS-Urban simulations for one central London grid-cell (for 27th August) with asurface temperature profile assigned based on SW simulations ($T_{Profile}$) and single facet ***T* (*T*$_{Single}$) and facet *T* range (*T*$_{Profile}$).** temperatures (T_{Single}), assessed using the normalised bias error (nBE, Eq. 8) for upwelling and downwelling clear-air fluxes ($LW_{\downarrow}$, $LW_{\uparrow}$), and the total outgoing and net flux into each urban facet (wall, roof, ground, e.g., $LW_{Out,Wall}$, LW^{*}_{Wall}).

Time	$LW_{\downarrow}$, z = 1		$LW_{\uparrow}$, z = H_{max}		LW^{*}_{Wall}	LW^{*}_{Roof}	LW^{*}_{Ground}	$LW_{Out,Wall}$	$LW_{Out,Roof}$	$LW_{Out,Ground}$
	$T_{Profile}$	*nBE* (%)	$T_{Profile}$	nBE (%)	nBE (%)	nBE (%)	nBE (%)	nBE (%)	nBE (%)	nBE (%)

Formatted: Font: Not Bold

Formatted: Font: Not Bold

Formatted: Font: Not Bold

Formatted: Font: Not Bold

Formatted: Font: Not Bold

7:45	11.0	0	29.0	0	-1.7	0.036	2.9	0.031	2.9	1.0
9:45	11.5	0	33.2	0	-1.9	0.063	1.2	-0.017	1.2	0.65
11:45	11.9	0	36.4	0	0.43	-0.072	-4.1	-0.12	-4.1	-1.2
13:45	12.0	0	36.7	0	-1.4	0.0045	-0.54	-0.11	-3.7	-1.1
17:45	11.7	0	31.1	0	-3.0	0.29	4.8	-0.054	-0.54	0.067

5 Comparison with the Harman et al. (2004) approach

Finally, SPARTACUS-Urban, DART and Harman et al. (2004)Harman et al. (2004) are applied to a case with an infinitely long canyon surrounded by buildings of equal height. The temperature configurations are used with the, with area-weighted SPARTACUS-Urban temperature profiles used in Harman approach (Eq. 7). For the more realistic temperature configurations, SPARTACUS-Urban single-layer and the Harman approach have similar run-times (Table 5). This increases by a factor of 10^2 s when realistic geometry is used in SPARTACUS-Urban. The full-temperature DART runs are 10^7 stimes slower than the most complex SPARTACUS-Urban simulations.

For simulations with each facet having a single surface temperature (cf. temperature profile), Harman et al. (2004) agrees better to DART $LW_{\uparrow}$ at the top-of canopy (H_{max}),For single surface temperatures per facet simulations (cf. temperature profile), $LW_{\uparrow}$ at the top-of canopy (H_{max}) Harman et al. (2004) is more similar to DART, with 5:45 UTC approximately equal (Figure 10). The poorest Harman - DART agreement to DART is for $LW_{In,Roof}$ and LW^*_{Wall}. Although, at 5:45 UTC, the nBE LW^*_{Wall} is approximately the same for SPARTACUS-Urban and Harman (Figure 10). This may be because no walls exist above $\overline{H}$, so roofs cannot intercept radiation from above, leading to an underestimate in $LW_{In,Roof}$. When DART hassimulations use a T range, the Harman performance is similar to the single facet T simulations (Figure 11). However, the nBE are generally higher, except for the LW^*_{Roof} and the LW_{Wall} fluxes (e.g., 13:45 UTC).

Formatted: Font: 9 pt

Generally, SPARTACUS-Urban agrees more closely to DART than Harman et al. (2004). In the varied facet T simulations, SPARTACUS-Urban and Harman approach are similar for $LW_{\uparrow}$, and $LW_{In,Roof}$, with nBE < 3%. The two models are similar for $LW_{Out,Ground}$ and $LW_{Out,Wall}$ throughout the day, with the smallest nBE (Figure SM 14, Figure SM 15). Largest differences are seen in the LW^*_{Ground} (SPARTACUS nBE 2-5% compared to Harman nBE > 20%), and in the LW^*_{Wall} (SPARTACUS nBE 0-10% cf. 8-16%).

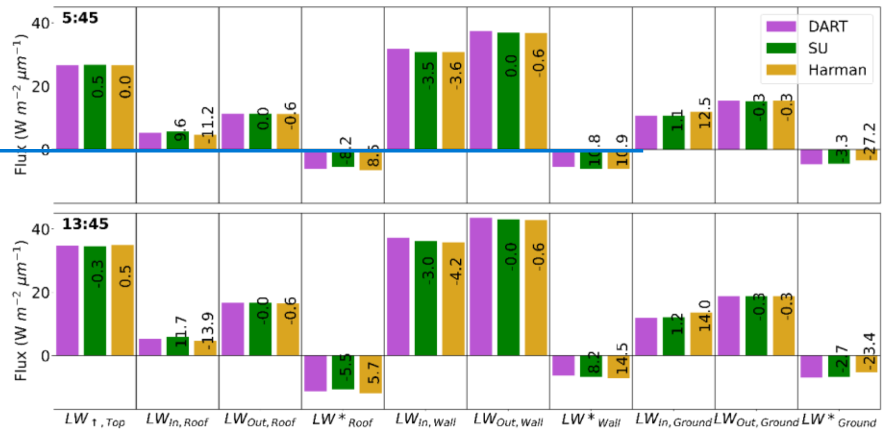

Generally, SPARTACUS-Urban agrees more closely to DART than Harman et al. (2004). In the varied facet *T* simulations, SPARTACUS-Urban and Harman approach are similar for $LW_{\uparrow}$ and $LW_{In,Roof}$, with nBE < 3%. The two models are similar for $LW_{Out,Ground}$ and $LW_{Out,Wall}$ throughout the day, with the smallest nBE (Figure SM 14-15). Largest differences are seen for LW^*_{Ground} (SPARTACUS nBE 2-5%, cf. Harman nBE > 20%) and LW^*_{Wall} (SPARTACUS nBE 0-10% cf. 8-16%).

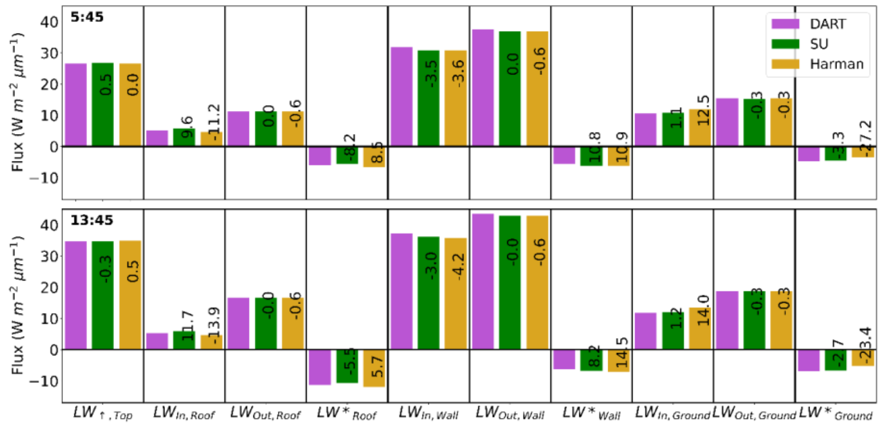

Figure 10: Comparison of simulations for one grid-cell in central London on 27th August using nBE (values, Eq. 8) relative to realistic world DART, for SPARTACUS-Urban (SU),) and Harman et al. (2004) longwave fluxes **for a real-world domain in central London, for an August day. Facet**with isothermal facet temperatures **are isothermal (prescribed as in** (Sect. 3.3): upwelling clear air flux at the top of the canopy ($LW_{\uparrow}$), and the roof, wall, and ground total interception, outgoing, and net flux, for two times (rows). **Numbers on each bar are the nBE (Eq. 7) between SPARTACUS-Urban/Harman approach and DART**

Formatted: Font: Not Bold
Formatted: Font: Not Bold
Formatted: Font: Not Bold
Formatted: Font: Not Bold
Formatted: Font: Not Bold
Formatted: Font: Not Bold
Formatted: Font: Not Bold
Formatted: Font: Not Bold

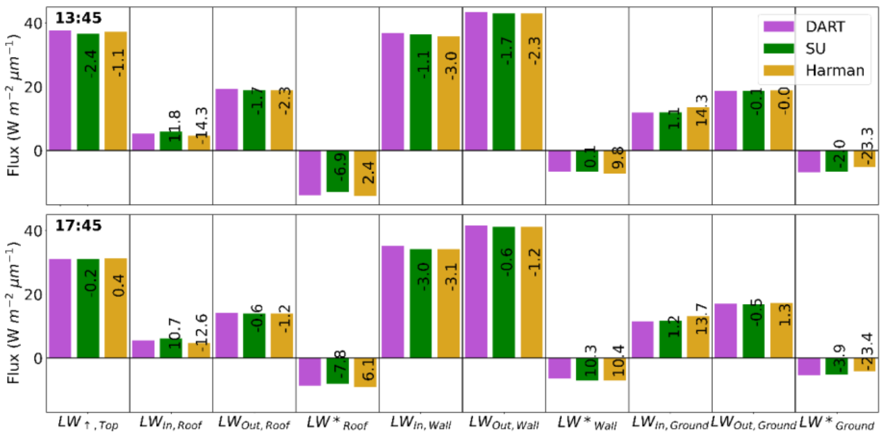

Figure 11: ~~As Figure 10 but~~ Comparison of simulations for one grid-cell in central London on 27th August using nBE (values, Eq. 8) relative to realistic world DART, for SPARTACUS-Urban (SU) and Harman et al. (2004) longwave fluxes with ~~facets temperature profile~~ facet temperatures prescribed based on SW simulations~~. DART: full T profile, Harman: area-weighted average of~~ (Sect. 3.3), upwelling clear air flux at the ~~SPARTACUS-Urban surface temperature profile.~~ top of the canopy ($LW_{\uparrow}$), and the roof, wall, and ground total interception, outgoing, and net flux, for two times (rows)

Table 5 Absolute run-time of Harman~~,~~ (Sect. 2.3), SPARTACUS-Urban~~,~~ (open-source version 0.7.3 compiled with gfortran, O3 optimization), and DART ~~with the indicated~~ (version 5.7.5 build number ~~of~~ 1126) for simulations with n vertical layers ~~(n),~~ and N diffuse streams per hemisphere ~~(N). Open-source SPARTACUS-Surface version 0.7.3 compiled with gfortran (O3 optimization). Runs~~. All runs undertaken in a ~~single-threaded~~ Linux environment on a dual Xeon E5-2667 v3 processor with 256 GB of RAM~~.~~, with a single-thread for Harman and SPARTACUS-Urban, but for DART ~~version 5.7.5 build number 1126 run in the same Linux environment with~~ 14 parallel threads using 32 CPU.

Model	n	N	Time (s)	Time relative to Harman
Harman	1	-	2 x 10^{-5}	-
SPARTACUS-Urban	1	8	3 x 10^{-5}	1.5
	6	8	4 x 10^{-4}	20
	151	1	2 x 10^{-3}	100
	151	4	2 x 10^{-3}	100
	151	8	2 x 10^{-3}	100
DART	151	-	6.6 x 10^{4}	3.3 x 10^{9}

6 Conclusions

Here, the longwave capabilities of the multi-layer radiative transfer model SPARTACUS-Urban are assessed using the explicit radiative transfer model, DART. DART resolves radiative interactions between individual facets of buildings, whereas SPARTACUS-Urban models the mean radiation field with height using building fraction and wall area at each height. Real-

Formatted
Formatted
Formatted
Formatted
Formatted
Formatted
Formatted
Formatted
Formatted
Formatted
Formatted
Formatted
Formatted
Formatted
Inserted Cells
Formatted
Formatted
Formatted
Formatted
Formatted
Formatted
Formatted
Formatted
Formatted
Formatted
Formatted
Formatted
Formatted
Formatted
Formatted
Formatted
Formatted
Formatted
Formatted
Formatted
Formatted
Formatted
Formatted
Formatted
Formatted
Formatted
Formatted
Formatted

world geometry is considered using prescribed categorised observed surface temperatures (*T*) ~~categorised from urban surface temperature observations~~ measured in London (Morrison et al. 2020, 2021).

Longwave (LW) fluxes are predicted well when one surface *T* is prescribed per facet type (or sub-facet, e.g., wall orientation). The clear-air upwelling and downwelling fluxes are predicted well, although there is some disagreement in the mid-canopy. SPARTACUS-Urban underestimates the net LW roof flux (normalised bias errors (nBE) -5.5 – -8.2~~%) the net LW roof flux,~~%), suggesting too much emission from surrounding walls. Errors in this configuration could be from the SPARTACUS-Urban geometry assumptions, or the wall-temperature averaging methods.

Similar agreement is found when facets are prescribed a temperature range based on shortwave simulations. The clear-air fluxes are in good agreement, with nBE ~~less than~~≤ 3% for all times assessed. The net wall LW is overestimated (nBE ~~up to~~≤ 10%) at times ~~when of~~with low intra-facet temperature variability (e.g., early morning and evening). Roof interception also is overestimated nearer the ground, leading to an underestimation in the net roof LW. However, all nBE < 11%. This suggests the average *T* profiles, informed by shortwave geometry are acceptable approximations of the true *T* field. However, we note the sub-facet wall *T* range is small, which may differ in different conditions (e.g. atmospheric, geometry).

SPARTACUS-Urban outperforms the frequently used infinite street canyon approach ~~(Harman et al. 2004) (cf.~~(Harman et al. 2004) (cf. DART). Both are similar if single *T* facets are used, except for the intercepted roof and net wall LW, when SPARTACUS-Urban is better. When using a facet temperature range the performance for both models is poorer. Harman notably underestimates roof interception, most likely linked to the absence of downward emission from walls higher in the canopy, given all are same height.

The impact of vertically varying *T* is small to SPARTACUS-Urban, with little impact on the net LW fluxes. However, only one summer day in central London is considered, possibly with small variations in wall *T*. In other geometries or climates (e.g., subtropical city with taller buildings), the impact of *T* profile (single, varied) application on the results still needs to be assessed and could be explored in future research.

~~Overall, this work suggests SPARTACUS-Urban's longwave fluxes agree well relative to the more complex, computationally and data demanding DART model. Alongside the evaluation of SPARTACUS-Urban for shortwave radiation (Stretton et al. 2022), good model performance is shown here, indicating it is suitable for implementing into a multi-layer urban model. Testing is underway with SPARTACUS-Urban coupled to the Surface Urban Energy and Water balance Scheme~~ Overall, this offline evaluation suggests SPARTACUS-Urban's longwave fluxes agree well relative to the more complex, computationally and data demanding DART model. Alongside the evaluation of SPARTACUS-Urban for shortwave radiation (Stretton et al. 2022), good model performance is shown here, indicating it is suitable for implementing into a multi-layer urban model.

Testing is underway with SPARTACUS-Urban coupled to the Surface Urban Energy and Water balance Scheme (SUEWS, Järvi et al. (2011, 2014); Ward et al. (2016); Omidvar et al. (2022), to predict the vertical profile of fluxes, surface temperatures, and heat stress metrics within the canopy. Such models require high resolution building geometry information (i.e., vertical descriptions of the urban canopy), which are unavailable for most cities. Therefore, to supplement these implementations an assessment should be made on how realistically available data influences model outputs, e.g., vertically distributed fluxes and temperatures.

Acknowledgments

The authors acknowledge the funding and support from the Scenario NERC Doctoral Training Partnership Grant, EPSRC 2130186, EPRSC DARE EP/P002331/1, ERC Synergy *urbisphere (855005)*, and Newton Fund/Met Office CSSP China NGC.

Data availability statement

The Fortran SPARTACUS-Surface package is available under an open-source license from https://github.com/ecmwf/spartacus-surface. The DART model is available from https://dart.omp.eu. All code and data used for this study are archived at 10.5281/zenodo.6798640

Competing interests

The contact author has declared that none of the authors has any competing interests

Author Contributions

MS performed the SPARTACUS-Urban simulations, data analysis, and wrote the initial manuscript. WM developed the 3D model), to predict the vertical profile of fluxes, surface temperatures, and heat stress metrics within the canopy, with future work including an online evaluation of SPARTACUS-Urban within SUEWS. Further, comparisons could be made between existing single- and multi-layer urban radiative transfer schemes, such as done in the RAMI intercomparison for vegetation (Widlowski et al. 2015), or urban energy balance intercomparisons (Grimmond et al. 2010, 2011; Lipson et al. 2023). Such models require high resolution building geometry information (i.e., vertical descriptions of the urban canopy), which are unavailable for most cities. Therefore, to supplement these implementations an assessment should be made on how realistically available data influences model outputs, e.g., vertically distributed fluxes and temperatures.

Acknowledgments

The authors acknowledge the funding and support from the Scenario NERC Doctoral Training Partnership Grant, EPSRC 2130186, EPRSC DARE EP/P002331/1, ERC Synergy *urbisphere* (855005), and Newton Fund/Met Office CSSP China NGC.

Data availability statement

The Fortran SPARTACUS-Surface package is available under an open-source license from https://github.com/ecmwf/spartacus-surface. The DART model is available from https://dart.omp.eu. All code and data used for this study are archived at 10.5281/zenodo.6798640

Competing interests

The contact author has declared that none of the authors has any competing interests

Author Contributions

MS performed the SPARTACUS-Urban simulations, data analysis, and wrote the initial manuscript. WM developed the 3D DSM, and performed the DART simulations with input from MS. RH is the main author of the SPARTACUS-Surface code, which was modified by MS. All authors designed the manuscript structure, read, and provided feedback on the manuscript. SG and RH formulated the initial idea. SG obtained for funding to support all except RH.

7 References

Aida, M., and K. Gotoh, 1982: Urban albedo as a function of the urban structure - A two-dimensional numerical simulation - Part II. *Boundary-Layer Meteorol.*, **23**, 415–424, https://doi.org/10.1007/BF00116270.

Antoniou, N., H. Montazeri, M. Neophytou, and B. Blocken, 2019: CFD simulation of urban microclimate: Validation using high-resolution field measurements. *Sci. Total Environ.*, **695**, 133743, https://doi.org/10.1016/J.SCITOTENV.2019.133743.

Ao, X., C. S. B. Grimmond, D. Liu, Z. Han, P. Hu, Y. Wang, X. Zhen, and J. Tan, 2016: Radiation fluxes in a business district of Shanghai, China. *J. Appl. Meteorol. Climatol.*, **55**, 2451–2468, https://doi.org/10.1175/JAMC-D-16-0082.1.

Blankenstein, S., and W. Kuttler, 2004: Impact of street geometry on downward longwave radiation and air temperature in an urban environment. *Meteorol. Zeitschrift*, **13**, 373–379, https://doi.org/10.1127/0941-2948/2004/0013-0373.

Bohnenstengel, S. I., S. Evans, P. A. Clark, and S. E. Belcher, 2011: Simulations of the London urban heat island. *Q. J. R. Meteorol. Soc.*, **137**, 1625–1640, https://doi.org/10.1002/QJ.855.

Chrysoulakis, N., and Coauthors, 2018: Urban energy exchanges monitoring from space. *Sci. Rep.*, https://doi.org/10.1038/s41598-018-29873-x.

Crum, S. M., and G. Darrel Jenerette, 2017: Microclimate variation among urban land covers: The importance of vertical and horizontal structure in air and land surface temperature relationships. *J. Appl. Meteorol. Climatol.*, **56**, 2531–2543, https://doi.org/10.1175/JAMC-D-17-0054.1.

Dissegna, M. A., T. Yin, H. Wu, N. Lauret, S. Wei, J. P. Gastellu-Etchegorry, and A. Grêt-Regamey, 2021: Modeling mean radiant temperature distribution in urban landscapes using dart. *Remote Sens.*, **13**, https://doi.org/10.3390/rs13081443.

Dou, J., and S. Miao, 2017: Impact of mass human migration during Chinese New Year on Beijing urban heat island. *Int. J. Climatol.*, **37**, 4199–4210, https://doi.org/10.1002/JOC.5061.

Evans, S., A. Hudson-Smith, and M. Batty, 2006: 3-D GIS; Virtual London and beyond: An exploration of the 3-D GIS experience involved in the creation of Virtual London. *CyberGeo*, **2006**, 1–20, https://doi.org/10.4000/cybergeo.2871.

Gaitani, N., I. Burud, T. Thiis, and M. Santamouris, 2017: High-resolution spectral mapping of urban thermal properties with Unmanned Aerial Vehicles. *Build. Environ.*, **121**, 215–224, https://doi.org/10.1016/j.buildenv.2017.05.027.

Gastellu-Etchegorry, J. P., and Coauthors, 2015: Discrete anisotropic radiative transfer (DART 5) for modeling airborne and satellite spectroradiometer and LIDAR acquisitions of natural and urban landscapes. *Remote Sens.*, **7**, 1667–1701, https://doi.org/10.3390/rs70201667.

Grimmond, C. S. B., and T. R. Oke, 1999: Aerodynamic Properties of Urban Areas Derived from Analysis of Surface Form. *J. Appl. Meteorol.*, https://doi.org/10.1175/1520-0450(1999)038<1262:APOUAD>2.0.CO;2.

Grimmond, C. S. B. B., and Coauthors, 2010: The International Urban Energy Balance Models Comparison Project: First Results from Phase 1. *J. Appl. Meteorol. Climatol.*, **49**, 1268–1292, https://doi.org/10.1175/2010JAMC2354.1.

Grimmond, C. S. B. B., and Coauthors, 2011: Initial results from Phase 2 of the international urban energy balance model comparison. *Int. J. Climatol.*, **31**, 244–272, https://doi.org/10.1002/joc.2227.

Guo, G., X. Zhou, Z. Wu, R. Xiao, and Y. Chen, 2016: Characterizing the impact of urban morphology heterogeneity on land surface temperature in Guangzhou, China. **84**, 427–439.

Hamdi, R., and V. Masson, 2008: Inclusion of a drag approach in the Town Energy Balance (TEB) scheme: Offline 1D evaluation in a street canyon. *J. Appl. Meteorol. Climatol.*, **47**, https://doi.org/10.1175/2008JAMC1865.1.

Harman, I. N., and S. E. Belcher, 2006: The surface energy balance and boundary layer over urban street canyons. *Q. J. R. Meteorol. Soc.*, **132**, 2749–2768.

——, M. J. Best, and S. E. Belcher, 2004: Radiative exchange in an urban street canyon. *Boundary-Layer Meteorol.*, **110**, 301–316, https://doi.org/10.1023/A:1026029822517.

Heaviside, C., H. Macintyre, and S. Vardoulakis, 2017: The Urban Heat Island: Implications for Health in a Changing Environment. *Curr. Environ. Heal. reports*, **4**, https://doi.org/10.1007/s40572-017-0150-3.

Hénon, A., P. G. Mestayer, J. P. Lagouarde, and J. A. Voogt, 2012: An urban neighborhood temperature and energy study from the CAPITOUL experiment with the Solene model: Part 2: Influence of building surface heterogeneities. *Theor. Appl. Climatol.*, **110**, 197–208, https://doi.org/10.1007/s00704-012-0616-z.

Hersbach, H., and Coauthors, 2020: The ERA5 global reanalysis. *Q. J. R. Meteorol. Soc.*, **146**, 1999–2049, https://doi.org/10.1002/QJ.3803.

Hertwig, D., H. L. Gough, S. Grimmond, J. F. Barlow, C. W. Kent, W. E. Lin, A. G. Robins, and P. Hayden, 2019: Wake Characteristics of Tall Buildings in a Realistic Urban Canopy. *Boundary-Layer Meteorol.*, **172**, 239–270, https://doi.org/10.1007/S10546-019-00450-7/TABLES/5.

——, and Coauthors, 2020: Urban signals in high-resolution weather and climate simulations: role of urban land-surface characterisation. *Theor. Appl. Climatol.*, **142**, 701–728, https://doi.org/10.1007/s00704-020-03294-1.

——, S. Grimmond, S. Kotthaus, C. Vanderwel, H. Gough, M. Haeffelin, and A. Robins, 2021: Variability of physical meteorology in urban areas at different scales: implications for air quality. *Faraday Discuss.*, **226**, 149–172, https://doi.org/10.1039/D0FD00098A.

Hilland, R. V. J., and J. A. Voogt, 2020: The effect of sub-facet scale surface structure on wall brightness temperatures at multiple scales. *Theor. Appl. Climatol.*, **140**, 767–785, https://doi.org/10.1007/s00704-020-03094-7.

Hogan, R. J., ~~2019~~2019a: Flexible Treatment of Radiative Transfer in Complex Urban Canopies for Use in Weather and Climate Models. *Boundary-Layer Meteorol.*, https://doi.org/10.1007/s10546-019-00457-0.

——, 2019b: An Exponential Model of Urban Geometry for Use in Radiative Transfer Applications. *Boundary-Layer Meteorol.*, https://doi.org/10.1007/s10546-018-0409-8.

Hogan, R. J., 2021: spartacus-surface. *GitHub Repos.*,.

Hogan, R. J., S. A. K. Schäfer, C. Klinger, J. C. Chiu, and B. Mayer, 2016: Representing 3-D cloud radiation effects in two-stream schemes: 2. Matrix formulation and broadband evaluation. *J. Geophys. Res.*, **121**, 8583–8599, https://doi.org/10.1002/2016JD024875.

——, T. Quaife, and R. Braghiere, 2018: Fast matrix treatment of 3-D radiative transfer in vegetation canopies: SPARTACUS-Vegetation 1.1. *Geosci. Model Dev.*, **11**, 339–350, https://doi.org/10.5194/gmd-11-339-2018.

Hu, L., and J. Wendel, 2019: Analysis of urban surface morphologic effects on diurnal thermal directional anisotropy. *ISPRS J. Photogramm. Remote Sens.*, **148**, 1–12.

Järvi, L., C. S. B. S. B. Grimmond, and A. Christen, 2011: The Surface Urban Energy and Water Balance Scheme (SUEWS): Evaluation in Los Angeles and Vancouver. *J. Hydrol.*, **411**, 219–237, https://doi.org/10.1016/j.jhydrol.2011.10.001.

——, C. S. B. Grimmond, M. Taka, A. Nordbo, H. Setälä, and I. B. Strachan, 2014: Development of the Surface Urban Energy and Water Balance Scheme (SUEWS) for cold climate cities. *Geosci. Model Dev.*, **7**, 1691–1711, https://doi.org/10.5194/gmd-7-1691-2014.

Kent, C. W., S. Grimmond, D. Gatey, and K. Hirano, 2019: Urban morphology parameters from global digital elevation models: Implications for aerodynamic roughness and for wind-speed estimation. *Remote Sens. Environ.*, **221**, 316–339, https://doi.org/10.1016/j.rse.2018.09.024.

Kershaw, S. E., and A. A. Millward, 2012: A spatio-temporal index for heat vulnerability assessment. *Environ. Monit. Assess.*, **184**, 7329–7342, https://doi.org/10.1007/S10661-011-2502-Z/FIGURES/5.

Kondo, A., M. Ueno, A. Kaga, and K. Yamaguchi, 2001: The influence of urban canopy configuration on urban albedo. *Boundary-Layer Meteorol.*, **100**, 225–242, https://doi.org/10.1023/A:1019243326464.

Kotthaus, S., T. E. L. Smith, M. J. Wooster, and C. S. B. S. B. Grimmond, 2014: Derivation of an urban materials spectral library through emittance and reflectance spectroscopy. *ISPRS J. Photogramm. Remote Sens.*, **94**, 194–212.

Kusaka, H., H. Kondo, Y. Kikegawa, and F. Kimura, 2001: A simple single-layer urban canopy model for atmospheric models:

Comparison with multi-layer and slab models. *Boundary-Layer Meteorol.*, **101**, 329–358, https://doi.org/10.1023/A:1019207923078.

Landier, L., J. P. Gastellu-Etchegorry, A. Al Bitar, E. Chavanon, N. Lauret, C. Feigenwinter, Z. Mitraka, and N. Chrysoulakis, 2018: Calibration of urban canopies albedo and 3D shortwave radiative budget using remote-sensing data and the DART model. *Eur. J. Remote Sens.*, https://doi.org/10.1080/22797254.2018.1462102.

Lee, S. H., and S. U. Park, 2008: A vegetated urban canopy model for meteorological and environmental modelling. *Boundary-Layer Meteorol.*, https://doi.org/10.1007/s10546-007-9221-6.

Lipson, M., and Coauthors, 2023: Evaluation of 30 urban land surface models in the Urban-PLUMBER project: Phase 1 results. *Q. J. R. Meteorol. Soc.*,.

Martilli, A., 2009: On the Derivation of Input Parameters for Urban Canopy Models from Urban Morphological Datasets. **130**, 301–306, https://doi.org/10.1007/s10546-008-9345-3.

——, A. Clappier, and M. W. Rotach, 2002: An Urban Surface Exchange Parameterisation for Mesoscale Models. *Boundary-Layer Meteorol.*, **104**, 261–304, https://doi.org/10.1023/A:1016099921195.

Masson, V., 2000: A Physically-Based Scheme For The Urban Energy Budget In Atmospheric Models. *Boundary-Layer Meteorol.*, **94**, 357–397, https://doi.org/10.1023/A:1002463829265.

——, 2006: Urban surface modeling and the meso-scale impact of cities. *Theor. Appl. Climatol.*, **84**, 35–45, https://doi.org/10.1007/s00704-005-0142-3.

Masson, V., and Coauthors, 2008: The Canopy and Aerosol Particles Interactions in TOulouse Urban Layer (CAPITOUL) experiment. *Meteorol. Atmos. Phys.*, **102**, 135–157, https://doi.org/10.1007/s00703-008-0289-4.

Meyn, S. K., and T. R. Oke, 2009: Heat fluxes through roofs and their relevance to estimates of urban heat storage. *Energy Build.*, **41**, 745–752, https://doi.org/10.1016/J.ENBUILD.2009.02.005.

Morrison, W., S. Kotthaus, C. S. B. Grimmond, A. Inagaki, T. Yin, J. P. Gastellu-Etchegorry, M. Kanda, and C. J. Merchant, 2018: A novel method to obtain three-dimensional urban surface temperature from ground-based thermography. *Remote Sens. Environ.*, **215**, 268–283, https://doi.org/10.1016/j.rse.2018.05.004.

——, T. Yin, N. Lauret, J. Guilleux, S. Kotthaus, J. P. Gastellu-Etchegorry, L. Norford, and S. Grimmond, 2020: Atmospheric and emissivity corrections for ground-based thermography using 3D radiative transfer modelling. *Remote Sens. Environ.*, **237**, https://doi.org/10.1016/j.rse.2019.111524.

——, S. Kotthaus, and S. Grimmond, 2021: Urban surface temperature observations from ground-based thermography: intra- and inter-facet variability. *Urban Clim.*, **35**, 100748, https://doi.org/10.1016/j.uclim.2020.100748.

Myint, S. W., E. A. Wentz, A. J. Brazel, and D. A. Quattrochi, 2013: The impact of distinct anthropogenic and vegetation features on urban warming. *Landsc. Ecol.*, **28**, 959–978, https://doi.org/10.1007/S10980-013-9868-Y/TABLES/5.

Nazarian, N., and J. Kleissl, 2015: CFD simulation of an idealized urban environment: Thermal effects of geometrical characteristics and surface materials. *Urban Clim.*, **12**, 141–159, https://doi.org/10.1016/J.UCLIM.2015.03.002.

Nunez, M., and T. R. Oke, 1977: ENERGY BALANCE OF AN URBAN CANYON. *J. Appl. Meteorol.*, https://doi.org/10.1175/1520-0450(1977)016<0011:TEBOAU>2.0.CO;2.

Oke, T. R., 1981: Canyon geometry and the nocturnal urban heat island: Comparison of scale model and field observations. *J. Climatol.*, **1**, 237–254, https://doi.org/10.1002/JOC.3370010304.

——, 1982: The energetic basis of the urban heat island. *Q. J. R. Meteorol. Soc.*, **108**, 1–24.

Oke, T. R., 1987: *Boundary layer climates, Second edition*.

Omidvar, H., and Coauthors, 2022: Surface Urban Energy and Water Balance Scheme (v2020a) in vegetated areas: parameter derivation and performance evaluation using FLUXNET2015 dataset. *Geosci. Model Dev.*, **15**, 3041–3078, https://doi.org/10.5194/GMD-15-3041-2022.

Ryu, Y. H., and J. J. Baik, 2012: Quantitative analysis of factors contributing to urban heat island intensity. *J. Appl. Meteorol. Climatol.*, **51**, https://doi.org/10.1175/JAMC-D-11-098.1.

Ryu, Y. H., J. J. Baik, K. H. Kwak, S. Kim, and N. Moon, 2013: Impacts of urban land-surface forcing on ozone air quality in the Seoul metropolitan area. *Atmos. Chem. Phys.*, **13**, 2177–2194, https://doi.org/10.5194/acp-13-2177-2013.

Schubert, S., S. Grossman-Clarke, and A. Martilli, 2012: A Double-Canyon Radiation Scheme for Multi-Layer Urban Canopy Models. *Boundary-Layer Meteorol.*, **145**, 439–468, https://doi.org/10.1007/s10546-012-9728-3.

Sobrino, J. A., C. Mattar, J. P. Gastellu-Etchegorry, J. C. Jiménez-Muñoz, and E. Grau, 2011: Evaluation of the DART 3D model in the thermal domain using satellite/airborne imagery and ground-based measurements. *Int. J. Remote Sens.*, https://doi.org/10.1080/01431161.2010.524672.

Souch, C., and S. Grimmond, 2006: Applied climatology: Urban climate. *Prog. Phys. Geogr.*, **30**, 270–279, https://doi.org/10.1191/0309133306PP484PR.

Stretton, M. A., W. Morrison, R. J. Hogan, and S. Grimmond, 2022: Evaluation of the SPARTACUS-Urban Radiation Model for Vertically Resolved Shortwave Radiation in Urban Areas. *Boundary-Layer Meteorol*~~. *2022*, 1–31.~~., **184**, 301–331, https://doi.org/10.1007/~~S10546~~s10546-022-00706-9.

Voogt, J. A., T. R. Oke, and T. O. JA Voogt, 1997: Complete urban surface temperatures. *J. Appl. Meteorol.*, **36**, 1117–1132, https://doi.org/10.1175/1520-0450(1997)036<1117:CUST>2.0.CO;2.

Ward, H. C., S. Kotthaus, L. Järvi, and C. S. B. Grimmond, 2016: Surface Urban Energy and Water Balance Scheme (SUEWS): Development and evaluation at two UK sites. *Urban Clim.*, **18**, 1–32, https://doi.org/10.1016/j.uclim.2016.05.001.

Widlowski, J. L., and Coauthors, 2015: The fourth phase of the radiative transfer model intercomparison (RAMI) exercise: Actual canopy scenarios and conformity testing. *Remote Sens. Environ.*, https://doi.org/10.1016/j.rse.2015.08.016.

Wu, J., Y. Zhou, Y. Gao, J. S. Fu, B. A. Johnson, C. Huang, Y. M. Kim, and Y. Liu, 2014: Estimation and uncertainty analysis of impacts of future heat waves on mortality in the Eastern United States. *Environ. Heal. Persp.*, **122**, 10–16, https://doi.org/10.1289/ehp.1308042r.

Zhang, J., C. K. Heng, L. C. Malone-Lee, D. J. C. Hii, P. Janssen, K. S. Leung, and B. K. Tan, 2012: Evaluating environmental implications of density: A comparative case study on the relationship between density, urban block typology and sky exposure. *Automation in Construction*.

715